Nagra
Nationale
Genossenschaft
für die Lagerung
radioaktiver Abfälle

Cédra
Société coopérative
nationale
pour l'entreposage
de déchets radioactifs

Cisra
Società cooperativa
nazionale
per l'immagazzinamento
di scorie radioattive

TECHNICAL REPORT 87-31

Crosshole Investigations – Physical Properties of Core Samples from Boreholes F1 and F2

K.-A. Magnusson
S. Carlsten
O. Olsson

June 1987

Swedish Geological Co, Sweden

Parkstrasse 23 5401 Baden/Schweiz Telephon 056/20 55 11

Nagra
Nationale
Genossenschaft
für die Lagerung
radioaktiver Abfälle

Cédra
Société coopérative
nationale
pour l'entreposage
de déchets radioactifs

Cisra
Società cooperativa
nazionale
per l'immagazzinamento
di scorie radioattive

TECHNICAL REPORT 87-31

Crosshole Investigations – Physical Properties of Core Samples from Boreholes F1 and F2

K.-A. Magnusson
S. Carlsten
O. Olsson

June 1987

Swedish Geological Co, Sweden

Parkstrasse 23 5401 Baden/Schweiz Telephon 056/20 55 11

Der vorliegende Bericht betrifft eine Studie, die für das Stripa-Projekt ausgeführt wurde. Die Autoren haben ihre eigenen Ansichten und Schlussfolgerungen dargestellt.Diese müssen nicht unbedingt mit denjenigen des Auftraggebers übereinstimmen.

Le présent rapport a été préparé pour le projet de Stripa. Les opinions et conclusions présentées sont celles des auteurs et ne correspondent pas nécessairement à ceux du client.

This report concerns a study which was conducted for the Stripa Project. The conclusions and viewpoints presented in the report are those of the authors and do not necessarily coincide with those of the client.

Das Stripa-Projekt ist ein Projekt der Nuklearagentur der OECD. Unter internationaler Beteiligung werden von 1980-86 Forschungsarbeiten in einem unterirdischen Felslabor in Schweden durchgeführt. Diese sollen die Kenntnisse auf folgenden Gebieten erweitern:
- hydrogeologische und geochemische Messungen in Bohrlöchern
- Ausbreitung des Grundwassers und Transport von Radionukliden durch Klüfte im Gestein
- Verhalten von Materialien, welche zur Verfüllung und Versiegelung von Endlagern eingesetzt werden sollen
- Methoden zur zerstörungsfreien Ortung von Störzonen im Fels

Seitens der Schweiz beteiligt sich die Nagra an diesen Untersuchungen. Die technischen Berichte aus dem Stripa-Projekt erscheinen gleichzeitig in der NTB-Serie der Nagra.

The Stripa Project is organised as an autonomous project of the Nuclear Energy Agency of the OECD. In the period from 1980-86, an international cooperative programme of investigations is being carried out in an underground rock laboratory in Sweden. The aim of the work is to improve our knowledge in the following areas:
- hydrogeological and geochemical measurement methods in boreholes
- flow of groundwater and transport of radionuclides in fissured rock
- behaviour of backfilling and sealing materials in a real geological environment
- non-destructive methods for location of disturbed zones in the rock

Switzerland is represented in the Stripa Project by Nagra and the Stripa Project technical reports appear in the Nagra NTB series.

Le projet Stripa est un projet autonome de l'Agence de l'OCDE pour l'Energie Nucléaire. Il s'agit d'un programme de recherche avec participation internationale, qui sera réalisé entre 1980 et 1986 dans un laboratoire souterrain, en Suède. Le but de ces travaux est d'améliorer et d'étendre les connaissances dans les domaines suivants:
- mesures hydrogéologiques et géochimiques dans les puits de forage
- chimie des eaux souterraines à grande profondeur
- écoulement des eaux souterraines et transport des radionucléides dans les roches fracturées
- comportement des matériaux de colmatage et de scellement des dépôt finals
- méthodes de localisation non destructive des zones de perturbation de la roche

La Suisse est représentée dans le projet Stripa par la Cédra. Les rapports techniques du projet Stripa sont publiés dans la série des rapports techniques de la Cédra (NTB).

ABSTRACT

The geology and physical properties has been studied of roughly 100 core samples from the boreholes F1 and F2 drilled at the Crosshole site, located at the 360 m level in the Stripa mine. The granitic rock has been divided into two classes: fracture zones (also called major units) and a rock mass which is relatively undeformed. Samples from the major units have lower resistivity, higher porosity and dielectric constant than the samples from the less deformed rock mass.

The electrical properties of the core samples have been measured over a frequency interval ranging from 1 Hz to 70 MHz. The conductivity of the samples increases with frequency, approximately with the frequency raised to the power 0.38. The dielectric constant decreases with frequency but is essentially constant above 3 MHz. These results show that the Hanai-Bruggeman equation can be used to describe the electrical bulk properties of the Stripa granite.

The electrical conductivity of the samples is well correlated to the water content of the samples. The granite has a small content$ of electrically conductive minerals which could influence the electrical bulk properties.

Key words: Granite, resistivity, porosity, dielectric constant, Hanai-Bruggeman equation.

RESUME

On a étudié la géologie et les propriétés physiques d'une centaine d'échantillons de carottes prélevés dans les forages F1 et F2, creusés sur le site d'essais entre puits, au niveau 360 m dans la mine de Stripa. On a divisé la roche granitique en deux types: les zones de fractures (appelées aussi unités majeures) et les zones de roches relativement peu déformées. Les échantillons provenant des unités majeures ont une résistivité plus basse, une porosité et une constante diélectrique plus élevées que celles calculées pour les zones de roches moins déformées.

Les propriétés électriques des échantillons de carottes ont été mesurées sur une intervalle de fréquences s'échelonnant entre 1 Hz et 70 MHz. La conductivité des échantillons augmente avec la fréquence, jusqu'à des valeurs de 0,38. La constante diélectrique baisse avec la fréquence mais est essentiellement constante au-dessus de 3 MHz. Ces résultats montrent que l'on peut employer l'équation de Hanai-Bruggeman pour décrire l'essentiel des propriétés électriques du granite de Stripa.

La conductivité électrique des échantillons correspond assez bien au contenu en eau des échantillons. Le granite a une faible teneur en minéraux électriquement conductifs, lesquels pourraient influencer la plupart des propriétés électriques.

ZUSAMMENFASSUNG

Rund 100 Kernproben aus den Bohrungen F1 und F2 des Crosshole-Gebietes, das sich auf der 360m-Sohle der Stripa-Mine befindet, wurden im Hinblick auf geologische und physikalische Eigenschaften untersucht. Das Granitgestein wurde in zwei Klassen unterteilt: 1. Störzonen (auch "major units" genannt) und 2. relativ homogenes Gestein. Proben aus den Störzonen zeigen niedrigere elektrische Widerstandswerte sowie höhere Porositäten und Dielektrizitätskonstanten als Proben aus dem relativ homogenen Gestein.

Die elektrischen Eigenschaften der Kernproben wurden im Frequenzbereich von 1 Hz bis 70 MHz bestimmt. Die Leitfähigkeit der Proben war abhängig von der Frequenz, potenziert mit Faktor 0,38. Die Dielektrizitätskonstante nimmt mit der Frequenz ab, bleibt aber ab ca. 3 MHz nahezu konstant. Diese Daten zeigen, dass die Hanai-Bruggeman-Gleichung zur Beschreibung der elektrischen Gebirgseigenschaften des Stripa-Granits benutzt werden kann.

Die elektrischen Leitfähigkeiten der Kernproben korrellieren gut mit dem Wassergehalt der Proben. Der Granit weist nur einen geringen Anteil elektrisch leitfähiger Mineralien auf, die die elektrischen Gebirgseigenschaften beeinflussen könnten.

Page

CONTENTS

SUMMARY

Samples have been taken from the core of the boreholes F1 and F2 at Stripa, 24 and 70 samples respectively. The samples were taken from major units (generally corresponding to fracture zones) and more undeformed rock.

The granite has a rather uniform density (mean 2 641 kg/m^3) and is practically unmagnetized (mean susceptibility 8.4 x 10^{-5} SI units, mean remanence 6.3 x 10^{-5} SI units). Induced polarisation is low and uniform (mean 1.56 %).

Thin sections prepared from 26 of the samples were investigated microscopically. The major units show strong deformation where microfractures and cavities occur frequently. The undeformed granite is more compact and has few microfractures and cavities. It can be considered as rather undeformed also on a microscopic scale.

The samples from the major units have a higher average porosity compared to the samples from the less deformed rock mass.

The major units have higher average porosity, electrical conductance and dielectric constant than the undeformed granite. Measurements were made both on saturated samples and dried samples. The soaked samples have considerably higher conductance and dielectric constant at lower frequencies than the dry rock samples. The difference becomes smaller at higher frequencies. The low frequency measurements exhibit lower values in resistivity than the high frequency measurements and in situ measurements.

Cross-plots in log-log scale of porosity vs resistivity for samples from the major units exhibit a more or less linear relation where the resistivity decreases with increasing porosity. The so called cementation factor in Archie's law is about 1.5.

The data presented in this study indicates that the Hanai-Bruggeman equation gives a rather good estimate of the porosity. The Hanai-Bruggeman equation gives the best result for the depolarisation factor 0.333 and for pore water conductivity and dielectric constant of about 0.1 S/m and 81, respectively.

There is very good correlation between physical properties of the Stripa granite, measured both in situ and on samples and the geological character observed both on microscopic scale and on macroscopic scale. The major units constitute the most porous and low resistive sections of the borehole, while the undeformed granite constitutes a uniform rock with low porosity and high resistivity, both in situ and on core samples.

most porous and low resistive sections of the borehole, while the undeformed granite constitutes a uniform rock with low porosity and high resistivity, both in situ and on core samples.

1. INTRODUCTION

Development of new methods for non-destructive site characterization has been the main task of the Crosshole Program of the Stripa Project. The research program has included development of radar, seismic, and hydraulic investigation methods and the application of these methods at the Crosshole site in the Stripa Mine. The radar and seismic methods have been developed with the objective to localize and characterize fracture zones and the results have then been compared with results from the hydraulic investigations. The comparison will be used to evaluate how well the geophysical methods can be used to predict the groundwater flow paths through crystalline rock.

In this context the borehole radar is a new investigation method which at the start of the project in 1983 had only been used to a very limited extent in crystalline. It was known from measurements on core samples that the electrical properties of rock were frequency dependant (Cook, 1975). In general the electrical conductivity increases with frequency and the dielectric constant decreases with frequency. The data available on the electrical properties at radar frequencies (10-500 MHz) were also scarce.

In order to be able to correlate radar responses observed in borehole measurements, such as reflections, variations in radar velocity and attenuation, samples were taken from the core from two boreholes at the Crosshole Site situated at the 360 m level in the Stripa Mine. Measurements have been made of the following properties;

- electrical conductivity
- dielectric constant
- porosity
- density
- magnetic susceptibility and remanence
- induced polarization

This report describes the results of these measurements. The physical properties of the core samples are compared to the geological characteristics of the samples. From this comparison inferences can be made of to what extent fracturing and different degrees of tectonization will affect radar waves.

2. DESCRIPTION OF THE CROSSHOLE SITE

This section gives a summary of the geological conditions of the Crosshole site. The summary is a compilation of the more comprehensive presentation of the geological and physical conditions of the Crosshole site given by Carlsten (1985) and Carlsten et. al., (1985).

The rock penetrated by the drillholes at the Crosshole site consists of so called Stripa granite. The drillholes intersect a few thin pegmatites, generally less than 0.1 m thick, one aplite 0.15 m thick, a single amphibolite 0.2 m thick and a few cm-thick quartz veins.

At the Crosshole site the Stripa granite contains several zones of tectonized rock, which exhibit various degrees of tectonization, ranging from slightly deformed rock to breccias. These zones constitute old scars in the bedrock which presently contain well healed coherent rock. Although these zones are well healed, they often contain cavities and are not as compact as the granite in general.

The boreholes at the Crosshole site penetrate several zones with tectonized rock. The zones with tectonized rock can in some cases occur as rather thin single isolated zones in wider sections with more undeformed granite. In general the zones form wider units with a complex pattern of tectonization. The degree of tectonization varies strongly across the units from slight red colouring to intense mylonitization and brecciation. The units are characterized by red colouring, alteration on fracture surfaces, and by several zones of breccia and mylonite. In association with the zones there are often cavities, filled or partly filled with idiomorphic crystals of calcite or fluorite. These units constitute the most intensely tectonized parts at the Crosshole site and were distinguished in each of the boreholes as "major units" in the description of the site given by Carlsten et. al., 1985. These so called major units have the most anomalous physical properties and therefore cause marked responses on several logs.

The specific geological and physical character of the major units enable idenfication of the units in several boreholes. Apart from two of the encountered major units in borehole F4 and F6, all the major units were correlated between the boreholes. The extension of these units was thereby followed over the Crosshole site. These six correlated major units are named A, B, C, D, E and F. It should be observed that unit B has only been

encountered in two of the boreholes F1 and F2. A less prominent unit, named unit 1, which intersects the boreholes a short distance from the front of the drift was also correlated between the boreholes. The radar measurements have traced another prominent zone through the Crosshole site, named K (Olsson et. al., 1987). The intersection of K in F4 and F6 coincides with the major units not previously correlated between the boreholes. For the position of the major units in each of the borehole, see Table 2.1.

Table 2.1 Position of the major units in the boreholes F1 - F6.

Unit	F1	F2	F3
1	12.3- 24.0	12.0- 26.0	13.2- 15.0
A	36.1- 39.4	42.0- 47.0	37.0- 41.0
B	95.5- 97.2	111.0-113.0	-
C	117.5-125.0	113.0-126.0	93.0-108.0
D	135.0-147.0	182.3-189.6	118.0-124.0
E	172.0-200.1	214.0-220.0	151.5-165.0
F	-	220.0-249.8	171.0-200.0
K	-	201.0-206.0	-

Unit	F4	F5	F6
1	12.0- 22.0	10.0- 17.0	12.0- 18.0
A	52.0- 55.0	36.0- 43.0	65.0- 71.0
B	-	-	-
C	100.0-110.0	90.0- 96.0	95.0-106.0
D	189.0-203.0	100.0-106.0	237.0-243.0
E	225.0-250.0	138.0-146.0	-
F	-	161.0-200.0	-
K	164.0-170.0	-	154.0-168.0

The major units constitute the most prominent weakness zones traced through the Crosshole site. These weakness zones separate the rock mass of the Crosshole site into smaller blocks of more undeformed rock mass between these zones. However, as mentioned before there also occur discrete separate tectonized zones such as breccia isolated in the wide sections of undeformed granite. These discrete zones are much more difficult to recognize in the adjacent boreholes and their extension could not be determined by correlation between the

boreholes. They are included in the rock mass and are not mapped as major units.

The major units have a similar strike which is NE-NNE and a steep dip towards ESE or WNW. Three of them, C and K and the less prominent unit 1, have a dip towards WNW and the rest of them towards ESE (Figure 2.1).

In some cases the brecciation found in the major units has been generated during different stages. For example the calcite healing in the unit C has in its turn been brecciated. It is evident that the healed zones constitute old scars in the bedrock which often can be reactivated during later deformation phases.

The deformed and healed zones probably are less competent compared to the more undeformed granite and therefore constitute zones which will be more easily fractured, i.e. they will not withstand stress as well as the undeformed rock. The major units therefore generally constitute the more fractured parts of the boreholes, but the degree of fracturing exhibits a large variation between the boreholes. Thus, the fracturing varies along the extension of the major units, i.e. some parts have withstood stress better than other parts. The TV-inspected fractures within the major units often have a dominating direction more or less subparallel to the extension of the units.

The fractures in more undeformed blocks of granite between the major units also have a dominating fracture direction in NNE and steep dip toward WNW or ESE, which is similar to those in the major units. Other fracture directions are more common in the undeformed granite, the NNE direction is not as dominating as in the major units. Also, this dominating fracture set is one of the most common fracture sets in the granite at other areas in the mine. It appears that a large proportion of the fractures are more or less subparallel to the major weakness zones found at the Crosshole site. The high degree of conformity of the fracturing and the extension of the major weakness zones can thus be an effect of the fact that later fracturing to a large extent follows old scars in the bedrock (Duran and Magnusson, 1984).

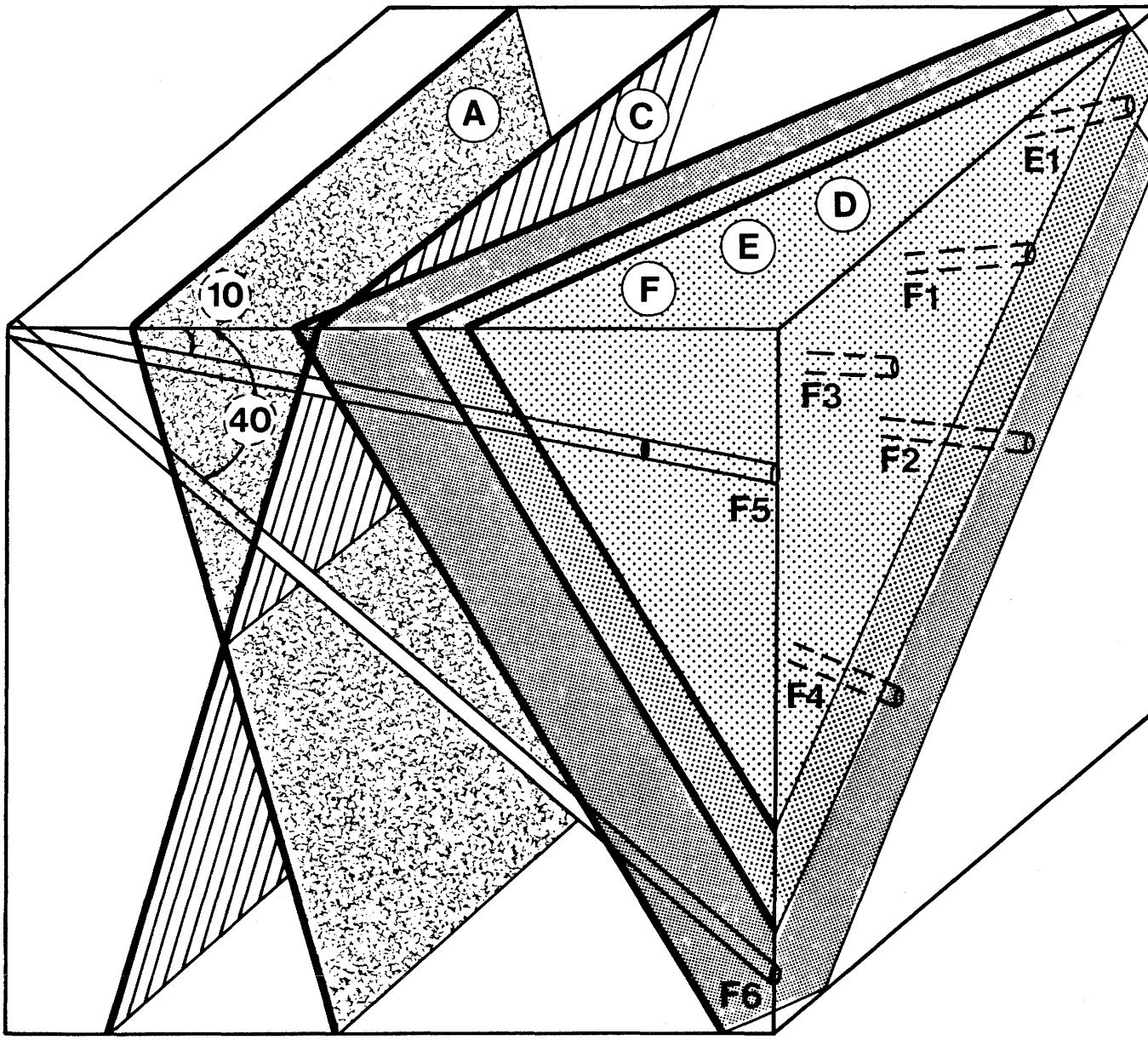

Figure 2.1 Block diagram showing the interpreted extension of the major units which have been correlated between the boreholes, excluding unit B. (from Carlsten et. al., 1985.)

3 SAMPLING

Samples have been taken from the cores of two 76 mm boreholes with 62 mm core diameter. The samples were cut in 40 mm long pieces. The two boreholes F1 (200 m in length) and F2 (250 m in length) have the same direction, 96° in the local mine coordinates, but different dips 10° and 20°, respectively. These two boreholes and the other so called fan boreholes (F3-F6) have been drilled from essentially the same position in the Crosshole site (Figure 3.1).

The total number of core samples collected from F1 and F2 is 24 and 70, respectively. From the more undeformed blocks of granite between the major units 6 samples were collected in F1, while 33 samples were collected in F2. The remaining samples were collected from the core sections within the major units, 18 in F1 and 37 in F2. The major unit C in F2 was sampled much more densly than the rest of the core, and 17 samples were taken from unit B and to the end of unit C. Note, unit B in F2 is situated very close to unit C (Figure 5.4 in Carlsten et. al., 1985). A few samples from the more undeformed granite were taken immediately outside the major units.

Unit C is a distinct and prominent unit encountered in all the fan boreholes, and was therefore chosen for a denser sampling in borehole F2. The samples were collected with a density of about 1.5 samples/m across both units B and C.

After measuring the physical properties at the SGAB laboratory the samples were sent to the Technical University of Luleå for determination of electrical properties using high frequency measurements. The size of the samples was too large for that equipment. The core samples were therefore cut to a length of 10 mm and the diameter was decreased to 31 mm by the use of a turning-lathe.

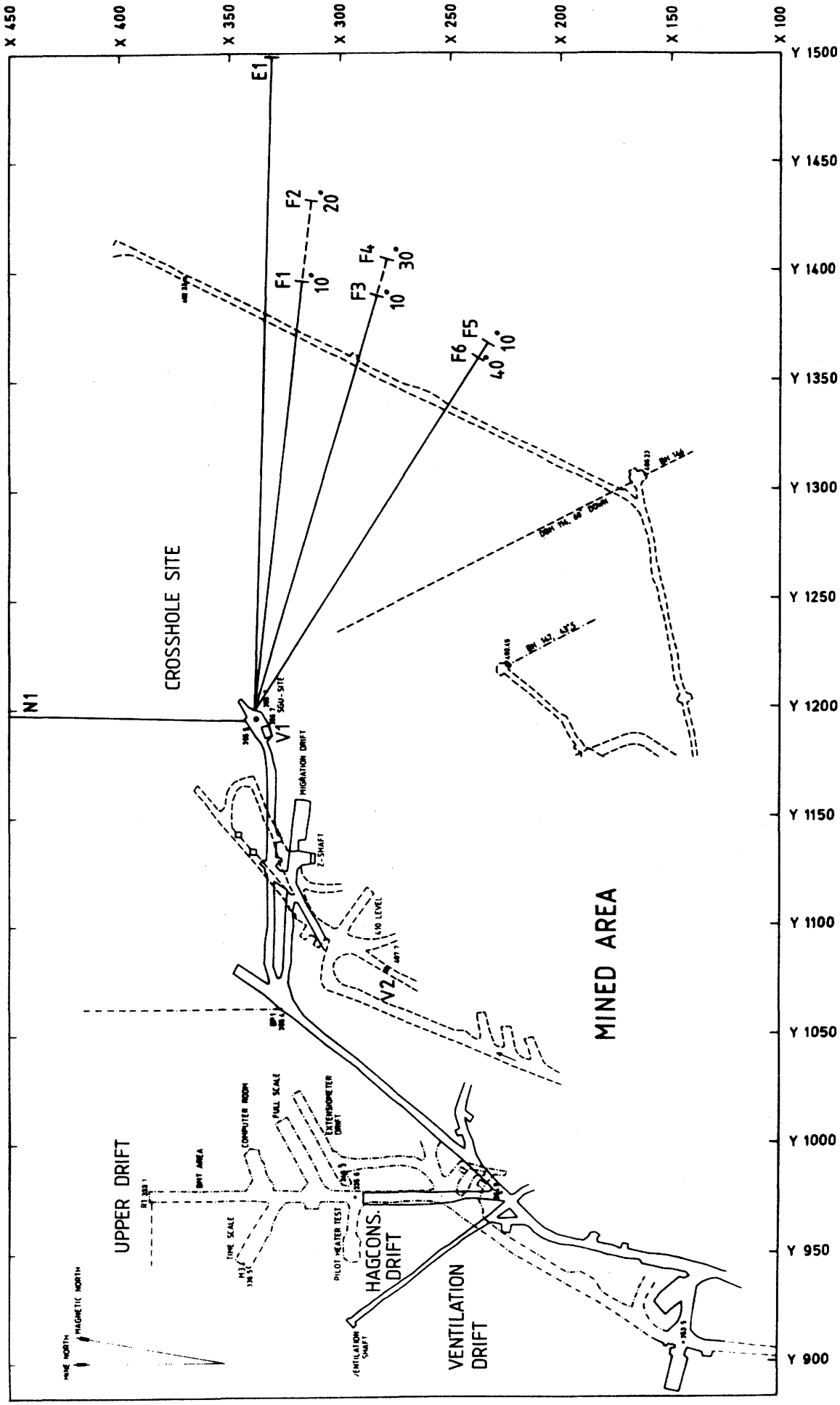

Figure 3.1 Plan view of the Stripa mine at the 360 m and 410 m levels showing the position of the boreholes at the Crosshole site.

4. PROPERTIES OF THE ROCK SAMPLES

Two of the measured physical properties, immersion porosity and resistivity, have been measured at both the laboratory of SGAB and the laboratory of the Technical University of Luleå. Both the laboratories used very similar measuring procedures. But to be able to use the equipment for high frequency measurements of the electrical properties at the laboratory of the Technical University it was necessary to decrease the size of the core samples. Although the same core samples have been measured the properties may be different after the change in size. The data on the physical properties of the core samples has been presented in a graduation work performed at the Technical University of Luleå (Ågmalm, 1985).

4.1 Porosity

The measured porosity is a so called immersion porosity where water is forced into the pores by a vacuum. Before refilling of the pores with water the samples were dried in an oven during 48 hours at 105^{o} C.

The dried samples were suspended above the water filled part of a vacuum desiccator under a pressure close to the vapor pressure of the water at room temperature. The pressure was maintained during 3 hours, after which the samples were dropped into the water and thereafter the pressure was rised. The samples were soaked in water during 50 hours (Öquist, 1981). The porosity of the samples was measured both on the core with 62 mm diameter at SGAB and on the core decreased in size (31 mm diameter) at the Technical University of Luleå. Both laboratories used the same measurement procedure.

Öquist (1981) has performed a study of the refilling of the pores of granite and granodiorite samples from Finnsjön. The samples were picked directly after the core had been taken up from the borehole and immediately enclosed in a container with water. After measurements of the density of water filled samples, they were dried and measured again, thereafter the samples were refilled and measured. The investigation shows that the average refilling is about 65 percent with a refilling range of 55-90 percent. By measuring mercury porosity and immersion porosity, Katsube (1981) has shown that the refilled water does not enter the sub-nanopores. He suggests that the sub-nanopores constitute about 50 percent or more of the total

porosity. This is in fair agreement with the percent of refilling of the Finnsjön samples.

Samples with anomalously high porosity occur within the major units, while the samples in the more undeformed rock have low uniform porosities. Note that the samples in the more undeformed rock immediately outside the major units also have low porosities (Figures 4.1 and 4.2).

The difference in porosities between the two measurements is probably an effect of the difference in sample size. Differences in sample size may cause a different degree of refilling and the reduction in size can also have an influence on the actual porosity of the sample. The smaller samples are to a lesser degree intersected by the coarser network of larger fractures, such as hairline fractures which can be seen in the samples.

The major unit named B in the description of the Crosshole site is characterized by containing cavities and constitutes an extremely porous granite (Carlsten et. al., 1985). It is more porous in borehole F1 and contains larger cavities than in F2 (Figures 4.1 and 4.2). It differs from the other major units which are characterized by tectonization, brecciation and mylonitization. Unit B is only encountered in F1 and F2 and therefore it does not constitute a zone of larger extension (Carlsten et. al., 1985).

The measured immersion porosity exhibits a clearly bimodal distribution of log normal type (Figure 4.3). The samples collected in the undeformed rock between the major units have a low average porosity of 0.25 percent and a standard deviation of $\pm$ 0.12. Note that the average and standard deviation are calculated from the logarithm of the porosity values. The samples collected within the major units, excluding B, exhibit a larger range of variation in porosity from values similar to those for the undeformed granite to porosity values up to 1 percent and larger. Thus, the major units have a higher logarithmic porosity average, 0.43 percent, and a larger standard deviation, $\pm$ 0.25.

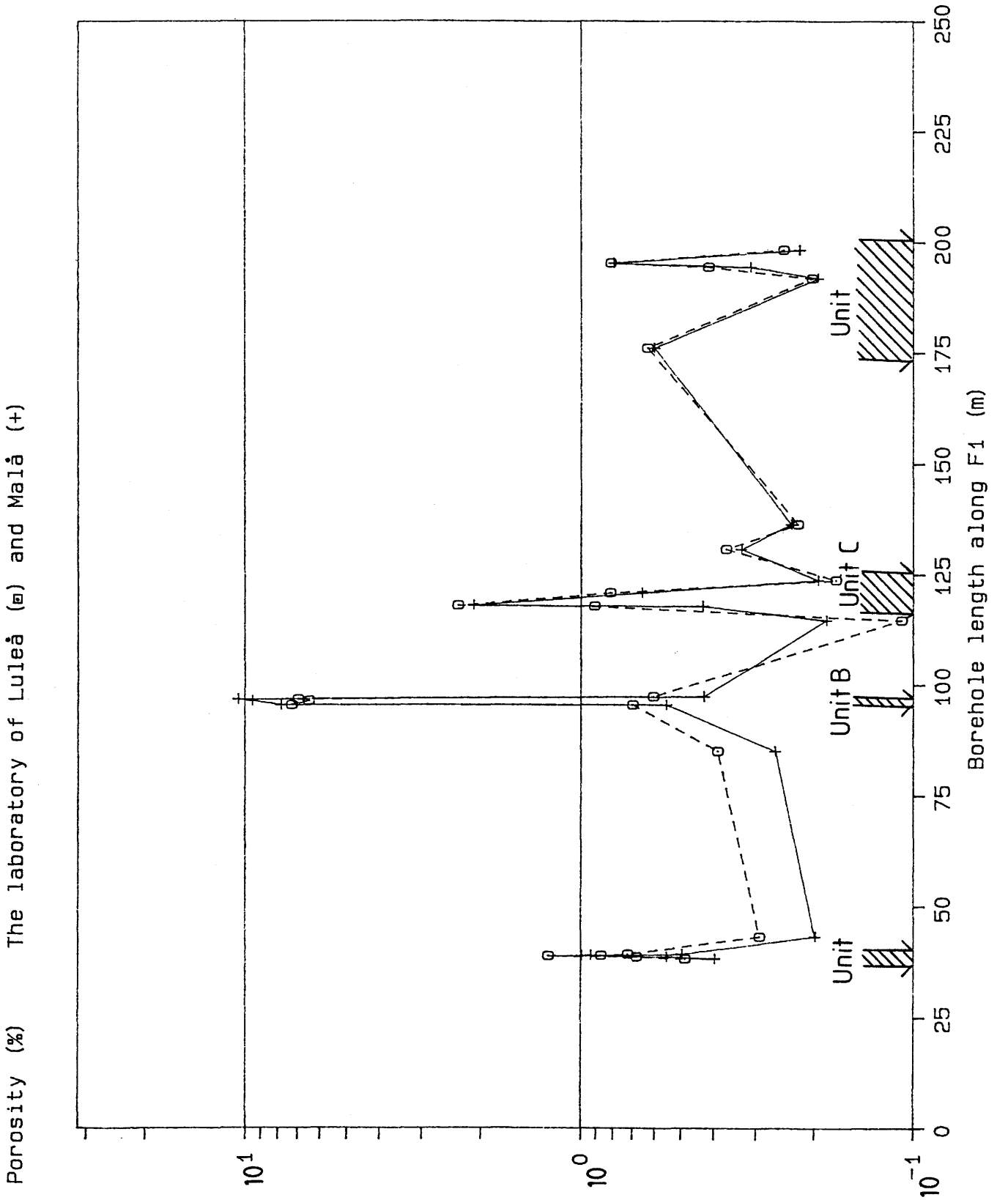

Figure 4.1 The measured immersion porosity of the samples along borehole F1, measured at the laboratory of SGAB (+) and the laboratory of the Technical University of Luleå (⊡). Note that the porosity is presented in a logarithmic scale.

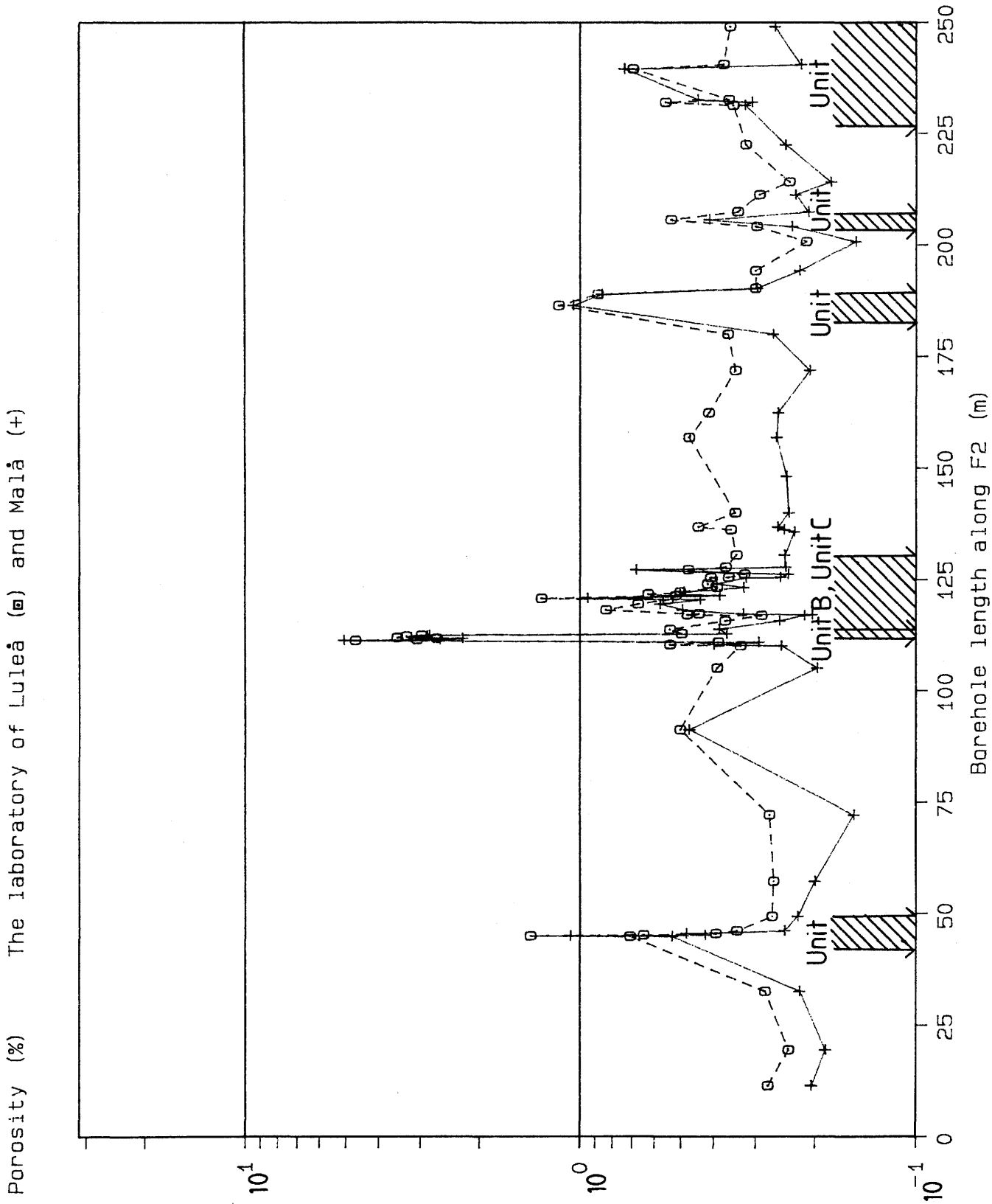

Figure 4.2 The measured immersion porosity of the samples along borehole F2, measured at the laboratory of SGAB (+) and the laboratory of the Technical University of Luleå (▣). Note that the porosity is presented in a logarithmic scale.

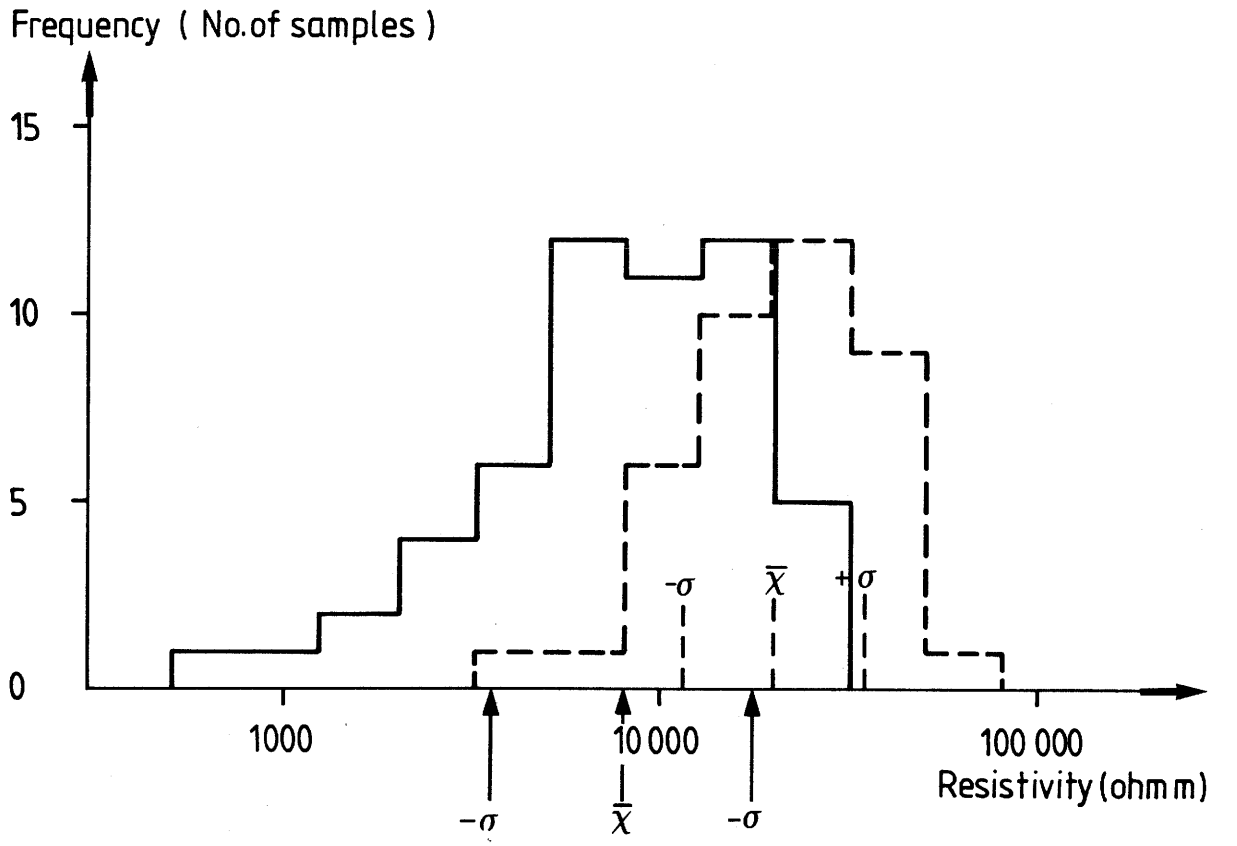

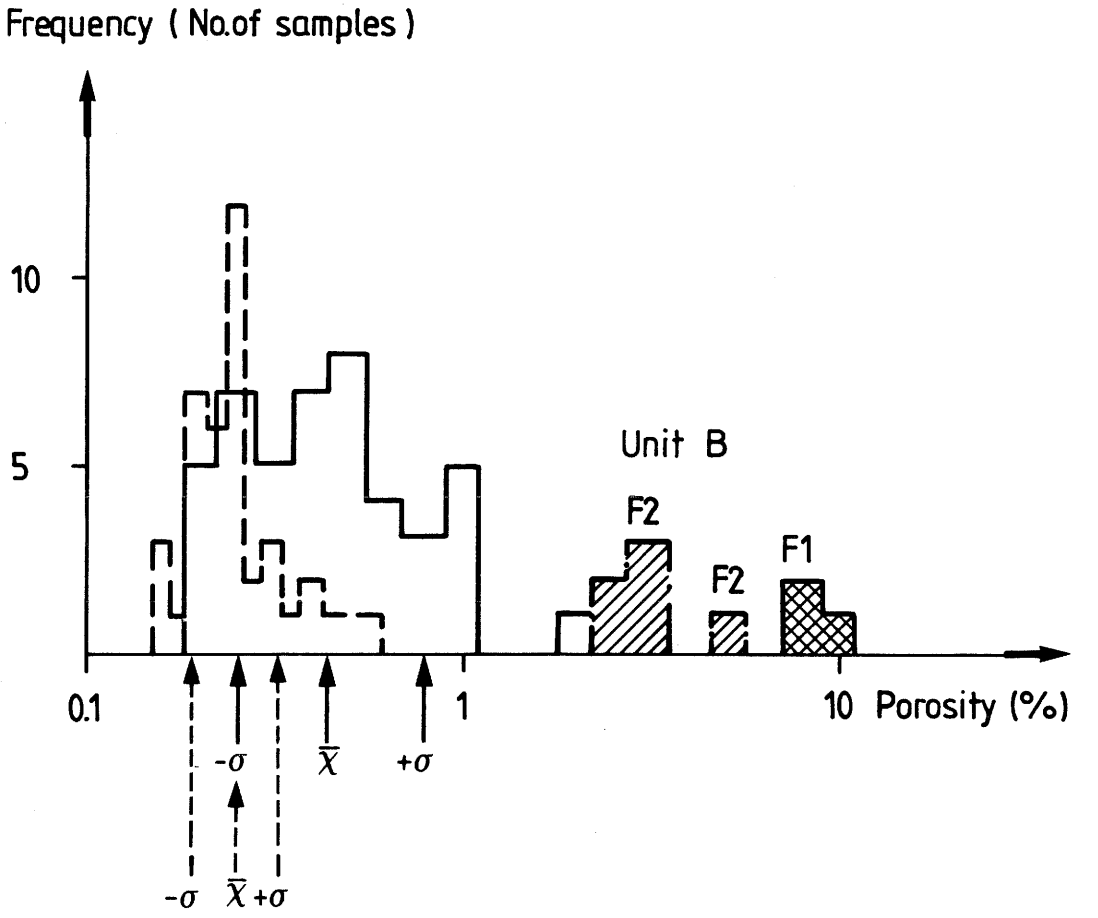

Figure 4.3 (a) Resistivity and (b) Porosity distribution of samples from the major units (solid line) and the undeformed granite (broken line). Hatched areas; samples from the porous unit B.

4.2 Resistivity measured at low frequency

After the samples had been soaked in tap-water (approx. 40 ohm-m) they were dried and thereafter inserted in a sample holder for measurements of both resistivity and induced polarization (IP). Each core sample is measured both along and across the core axis. The sample holder consists of a pair of collars of plexiglass, each containing a current and a potential electrode made of copper. Since the current and potential electrodes are electrically connected, this system is called the "two electrode system". The system works at a frequency of 1 Hz. The measuring method is described in detail by Öquist (1981).

The resistivity measurement is influenced by the humidity of the room and the dryness of the sample surface. When a resistivity measurement is made at some unspecified moment there is an uncertainty in the determination of the resistivity due to the evaporation from the sample surface which generally amounts to a factor 2 to 5 (Öquist, 1981). These measurements will therefore not give the true resistivity of the samples but rather a picture of the variation in resistivity.

The resistivity of the samples exhibits a similar pattern as the porosity, where the samples with anomalously low resistivity occur within the major units, while the samples in the more undeformed granite have a higher average resistivity (Figures 4.4 and 4.5).

The distribution of the resistivity of the samples was divided into samples within the major units and samples in the more undeformed granite. The samples in the undeformed granite exhibit a log normal distribution with a logarithmic average of 20 kohm-m and a standard deviation of ± 0.24. The samples collected within the major units exhibit a larger range of resistivity values from almost as high as those of the undeformed granite to resistivities below 1000 ohm-m. Thus, the major units have a lower logarithmic resistivity average of 7 700 ohm-m and a larger standard deviation of ± 0.35. (Figure 4.3).

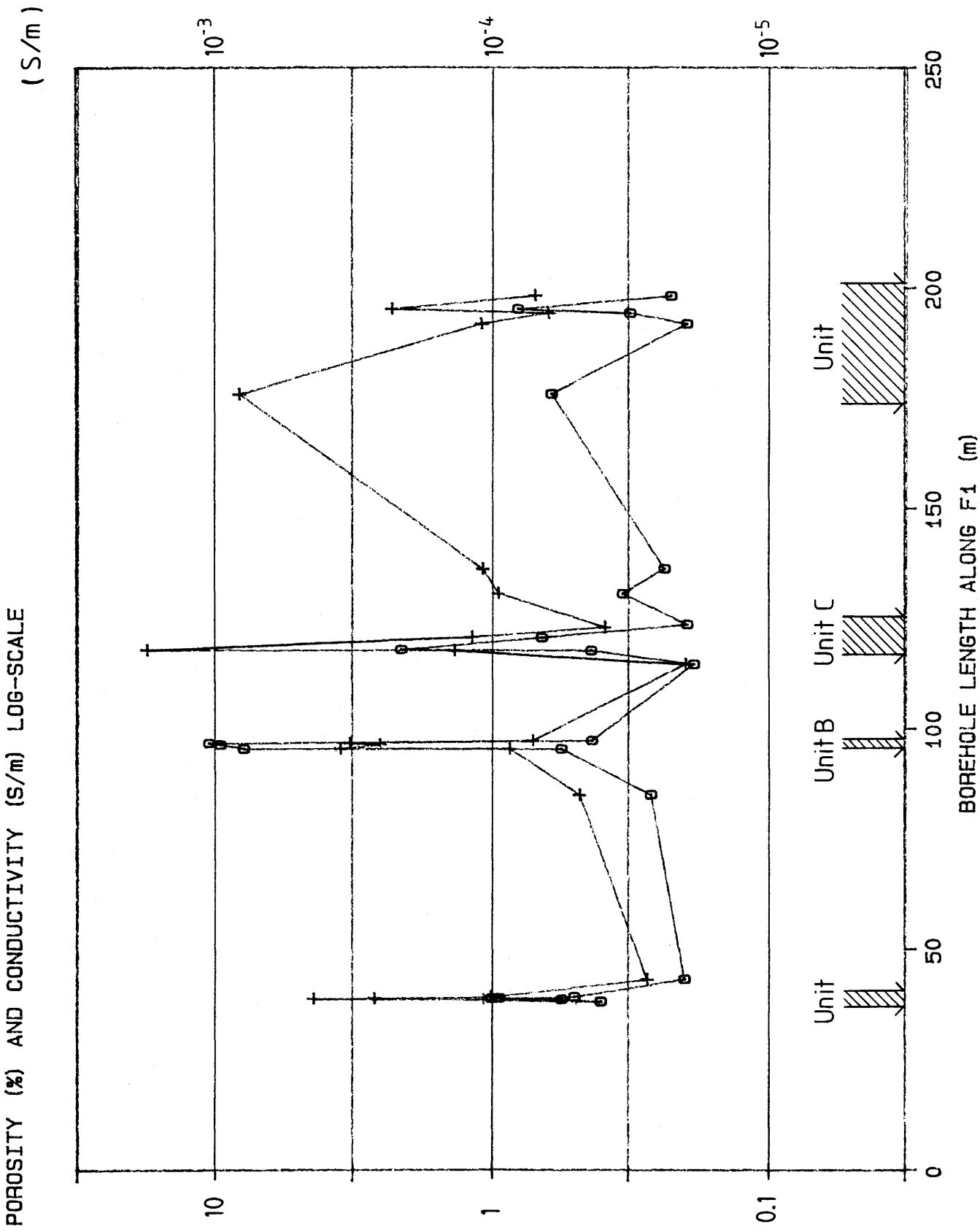

Figure 4.4 The measured immersion porosity (⊡) and resistivity (+) (measured at low frequency 1 Hz) of the samples along F1, measured at the laboratory of SGAB.

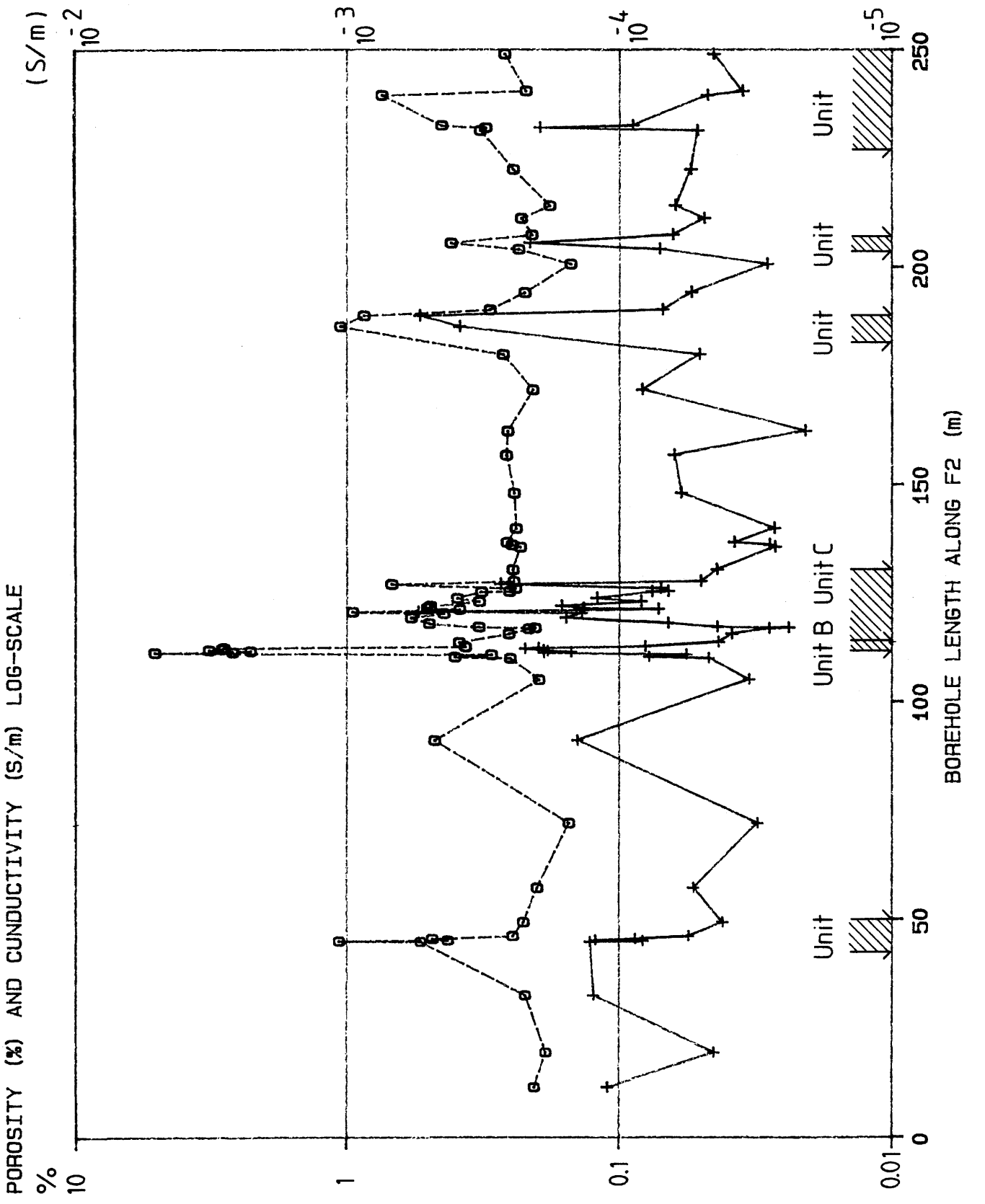

Figure 4.5 The measured immersion porosity (⊡) and resistivity (+) (measured at low frequency 1 Hz) of the samples along F2, measured at the laboratory of SGAB.

4.3 Density, magnetic properties and IP-effect

The granite, excluding unit B, has a rather uniform density with a mean value of 2 641 kg/m^3 and a standard deviation of ±23 kg/m^3. The extremely high porosity of unit B results in an anomalously low density (Figure 4.6).

The measured core samples have very low magnetization, both susceptibility and remanence. The granite is practically unmagnetized and has a susceptibility with a logarithmic average of about 8.4 x 10^{-5} (SI units) ±0.16 and a remanence with a logarithmic average of 6.3 x 10^{-5} (SI units) ±0.14. The two samples characterized by higher magnetization are collected from two breccias (Figure 4.7). The susceptibility logging of the boreholes at the Crosshole site show that minor increases of the suceptibility occur at some of the breccias and mylonites. The increased susceptibility is probably caused by an increased content of mafic paramagnetic minerals (Carlsten et. al., 1985).

The samples show that the penetrated rock has a low and uniform induced polarization with a mean value of 1.56 percent and a standard deviation of ±0.39 percent (Figure 4.8). The IP-effect is not influenced by the difference between major units and undeformed granite.

4.4 Microscopic study of thin sections

Thin sections were prepared from 26 of the collected core samples from F1 and F2. Seven of these samples were collected from the undeformed granite between the major units (Table 4.1) and 19 samples were collected within the major units (Table 4.2).

The undeformed granite is on a microscopic scale characterized by large grains of feldspar and quartz. In the microscopic study quartz shows evidence of stress by having undulatory extinction, but the grains are generally not fractured. Feldspar grains are often clear, but in some cases these grains exhibit a minor degree of sericitization. Large grains of muscovite occur frequently and in some cases they exhibit deformation into bent shapes. Also, hornblende alteration generally is associated with muscovite grains. Accessory minerals are opaque minerals, garnet and zircon. Microfractures in this undeformed granite do occur, but not in a large amount and usually they occur in association with grain boundaries and they do not penetrate separate grains (Tables 4.1 and 4.3).

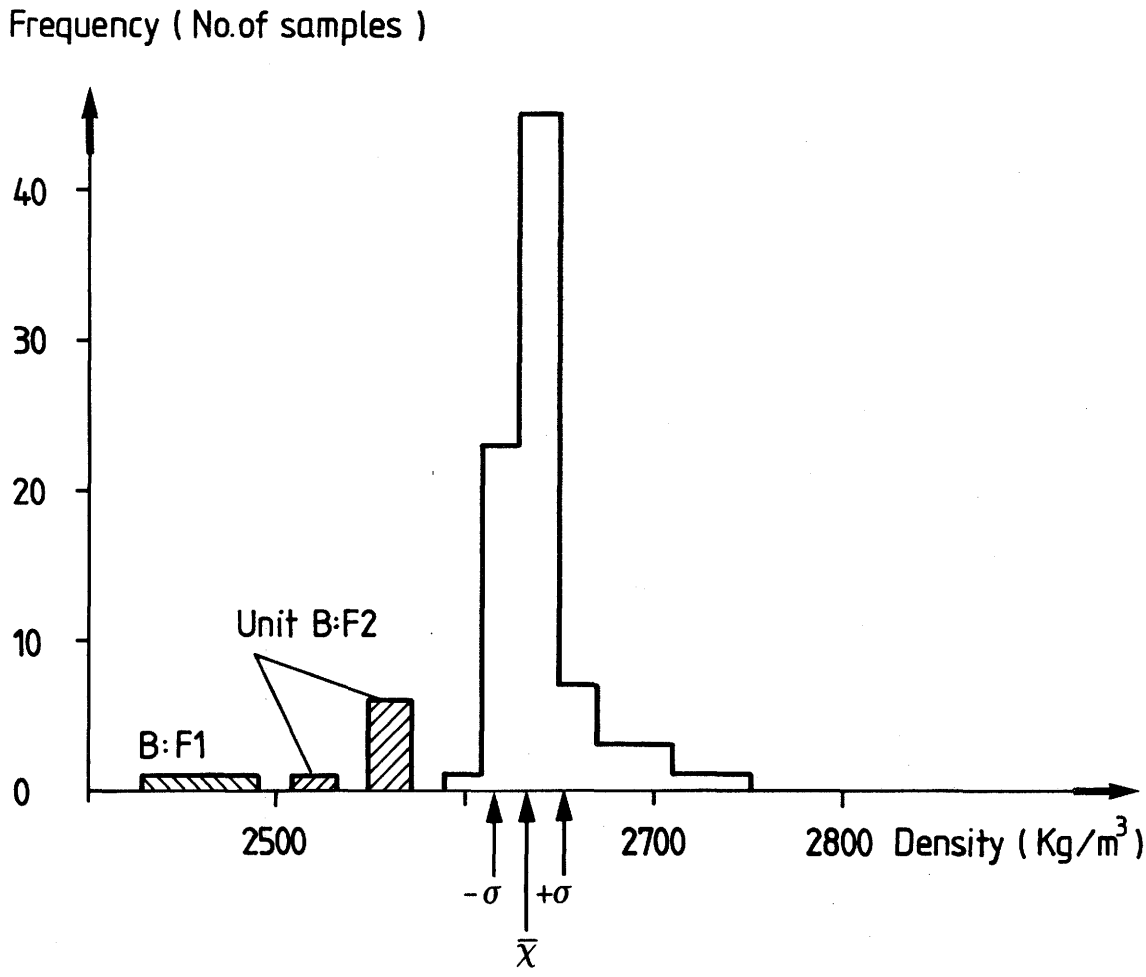

Figure 4.6 Density distribution of all measured samples. Hatched areas samples from the porous unit B.

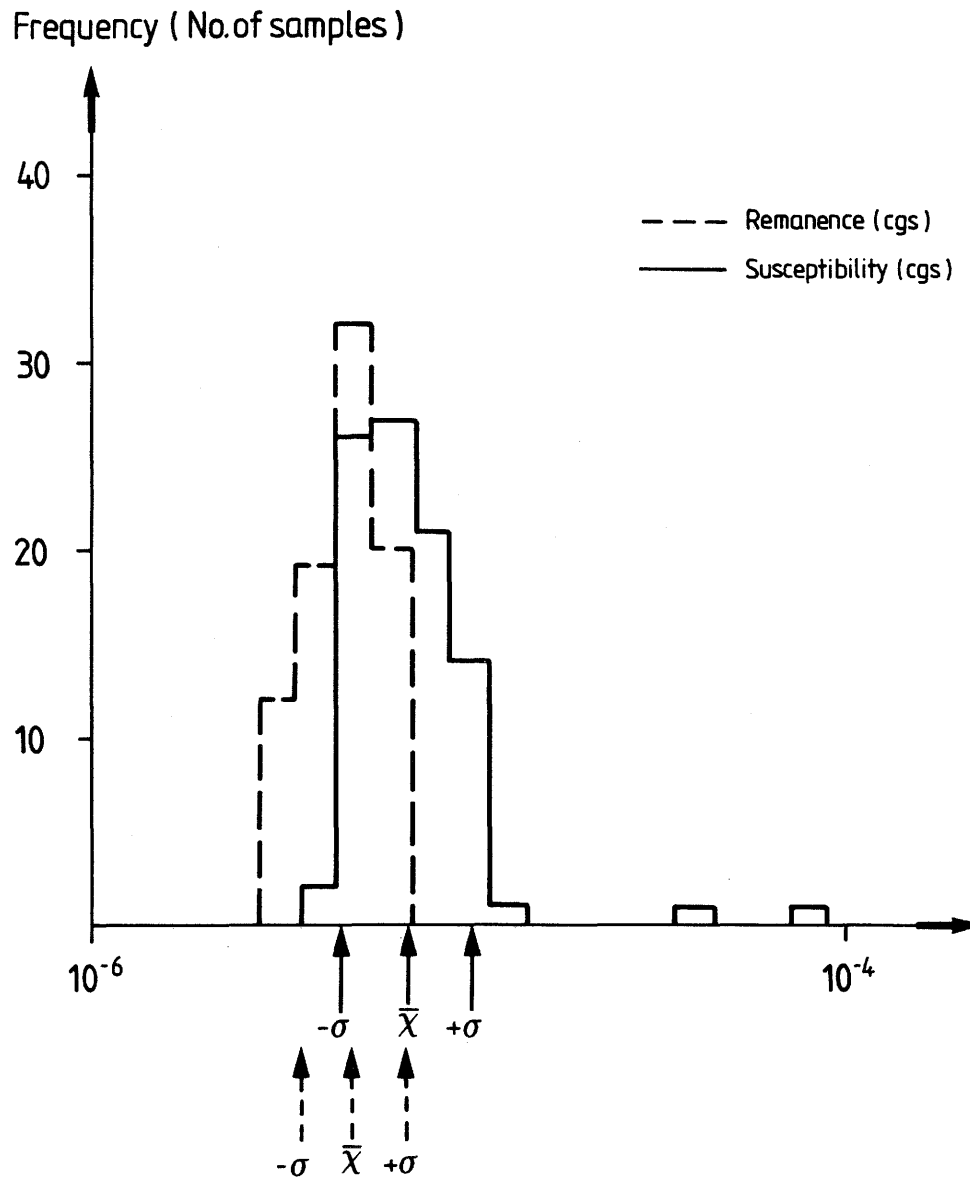

Figure 4.7 Distribution of susceptibility and remanent magnetization of all samples.

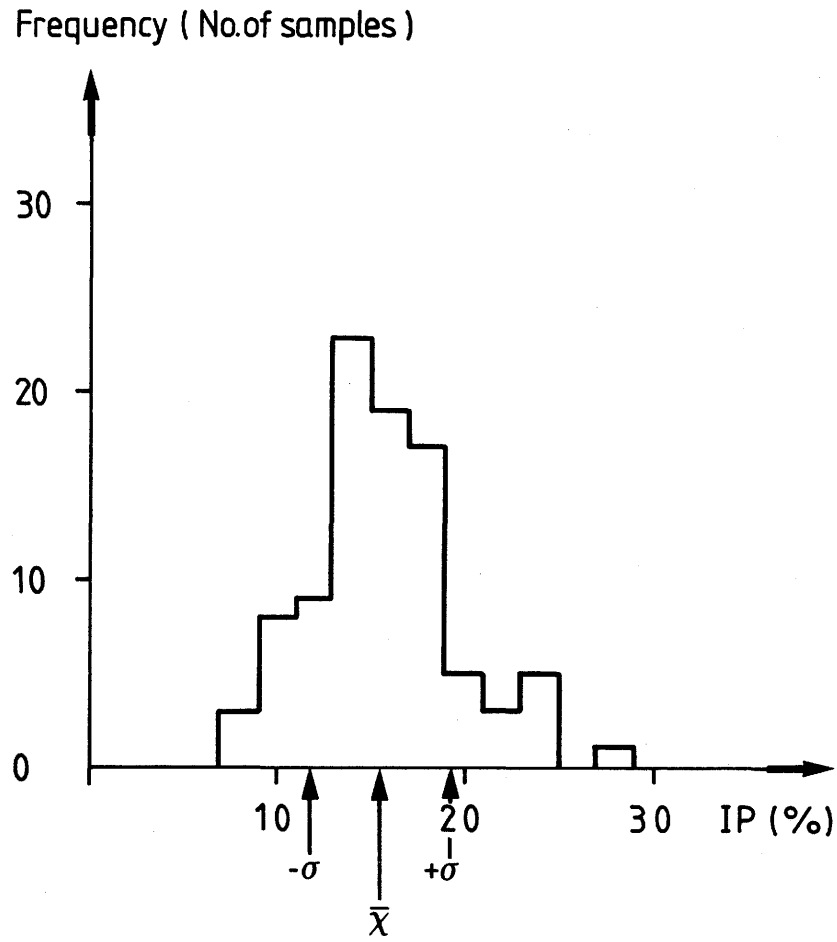

Figure 4.8 Distribution of the induced polarization of all samples.

The granite within the major units shows clear evidence of strong deformation in microscopic scale as well as in the macroscopic scale, which is described in Chapter 2. The grain matrix differs by being more granular and with grain sizes several times smaller than the undeformed granite. Quartz is strongly stressed and fractured into smaller separate grains. The feldspar grains are also fractured and cloudy due to the fact that strong sericitization is common. Brecciation is also evident in microscopic scale by the frequent occurence of microbreccias (Tables 4.2 and 4.4). The microbreccias constitute rock crushed into fragments which are cemented and healed together by a very finely grained matrix. The very fine texture of the matrix makes it difficult to identify the minerals, but it is evident that calcite healing is a common feature (Figure 4.9). Cavities occur rather frequently in association with the microbreccias. These microbreccias cut through the grains and can be followed across the thin sections. They can have very different widths as can be seen in the photographs of the thin sections, Figure 4.9 a wider microbreccia, and Figure 4.10 a thin microbreccia.

Microfractures occur frequently and often cut through and dislocate grains (Figure 4.11). There also appear wide fractures with coarse calcite healing accompanied by fluorite (Figure 4.12). Open microfractures can be observed in the thin sections. It has also been observed that the more or less parallel set of microfractures is oriented parallel to microbreccias, which is in agreement with observations on a macroscopic scale where a large proportion of the fractures are more or less subparallel to the extension of the major units (Carlsten et. al., 1985).

In general the characteristic features of the major units such as massive calcite-fluorite healing of both fractures and breccias, the fracturing and cavities can be observed both in microscopic and macroscopic scale. The pattern of deformation is thus similar both in microscopic and macroscopic scale.

Table 4.1 Microscopic study of thin sections within the major units.

Sample		1	2	3	4	5	6	7	8	9
F1:1	T	x	x		x	x		x	x	x
F1:3	B	x	x	x	x	x			x	
F1:4	B	x	x	x	x	x			x	
F1:15	B	x	x		x	x			x	x
F1:16	B	x	x		x		x	x	x	x
F1:20	T	x	x		x				x	x
F1:25	T				x	x		x	x	x
F2:2	T				x					x
F2:30	T	x	x		x	x				x
F2:32	T	x	x	(x)	x		x	(x)		x
F2:35	T	x	x		x				x	(x)
F2:39	T	(x)			x			x		x
F2:40	T	x			x		x	x		x
F2:41	T	x	x		x				x	x
F2:53	B	x	x		x			(x)	(x)	x
F2:54	B	x	x		x	x			(x)	
F2:60	T	x	x		x					
F2:69	B	x	x		x				x	(x)
F2:70	T	x	x		x	x			x	x

1. Microbreccia
2. Calcite healing
3. Fluorite healing
4. Microfractures
5. Quartzhealed fractures
6. Evengrained
7. Large muscovite crystals
8. Open fractures
9. Sericitization

T. Sample from tectonized section.
B. Sample from brecciated section.
(x) Feature not strong.

Table 4.2 Microscopic study of thin sections in the more undeformed granite between the major units.

Sample	1	2	3	4	5	6	7	8	9
F1:6						x	x		(x)
F1:7						x	(x)		
F1:13		x	x	x		x			
F2:3						x	x		(x)
F2:11						x	x		x
F2:13	x	x		x		x	x		x
F2:48						x	x		x

1. Microbreccia
2. Calcite healing
3. Fluorite healing
4. Microfractures
5. Quartzhealed fractures
6. Evengrained
7. Large muscovite crystals
8. Open fractures
9. Sericitization

(x) Feature not strong.

Table 4.3 Microscopic study of detailed features of microfractures and microbreccias within the major units.

Sample	1	2	3	4	5	6	7
F1:1 T	x			x	x	x	x
F1:3 B	x			x	x	x	x
F1:4 B	x			x	x	x	
F1:15 B	x			x	x	x	x
F1:16 B	x			x		x	x
F1:20 T	x			x	x	x	x
F1:25 T	x		x		x		
F2:2 T		x	x				
F2:30 T	x		x	x		x	
F2:32 T	x		x	x		x	
F2:35 T	x			x	x	x	
F2:39 T		x	x	x			
F2:40 T	x		x	x		x	
F2:41 T	x		x	x		x	x
F2:53 B	x		x	x		x	(x)
F2:54 B	x		x	x		x	(x)
F2:60 T	x		x	x		x	
F2:69 B	x			x	x	x	
F2:70 T	x			x	x	x	

1. Crosscutting microfractures.
2. Microfractures along grain boundaries.
3. Very thin microfractures.
4. Visible infilling in microfractures.
5. Open microfractures.
6. Crosscutting microbreccias.
7. Open microbreccias.

T. Sample from tectonized section.
B. Sample from brecciated section.
(x) Feature not strong.

Table 4.4 Microscopic study of detailed features of microfractures and microbreccias in the more undeformed rock between the major units.

Sample	1	2	3	4	5	6	7
F1:6		x	x				
F1:7		x		x			
F1:13	x	x	x	x			
F2:3							
F2:11		x	x				
F2:13	x			x		x	
F2:48		x	x				

1. Crosscutting microfractures.
2. Microfractures along grain boundaries.
3. Very thin microfractures.
4. Visible infilling in microfractures.
5. Open microfractures.
6. Crosscutting microbreccias.
7. Open microbreccias.

(x) Feature not strong.

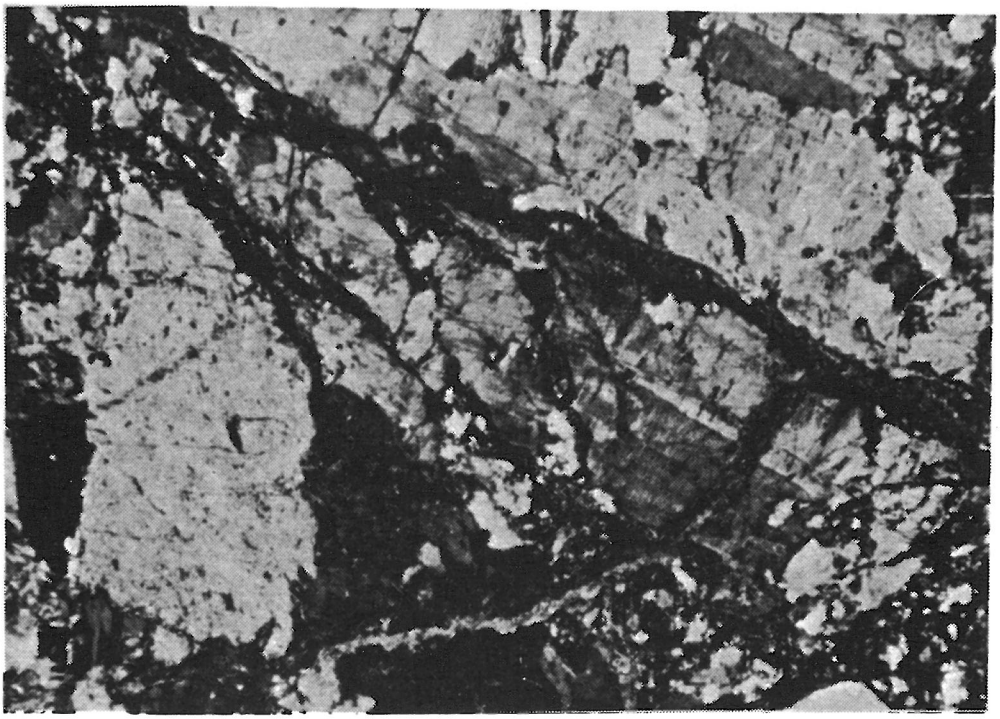

Figure 4.9 Brecciated section with sealed fractures. Area of the picture is 1.9 x 2.6 mm. Crossed Nicols.

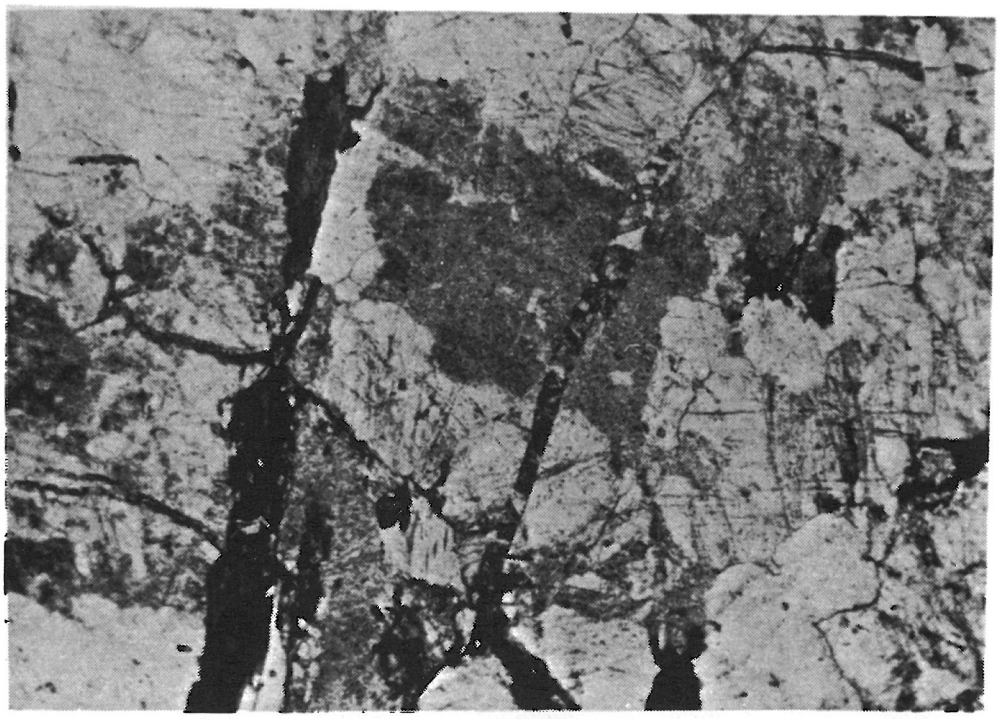

Figure 4.10 Fractures sealed by calcite, partly open. A thin brecciated fracture crosscut the thin section. Area of the picture is 1.9 x 2.6 mm. Crossed Nicols.

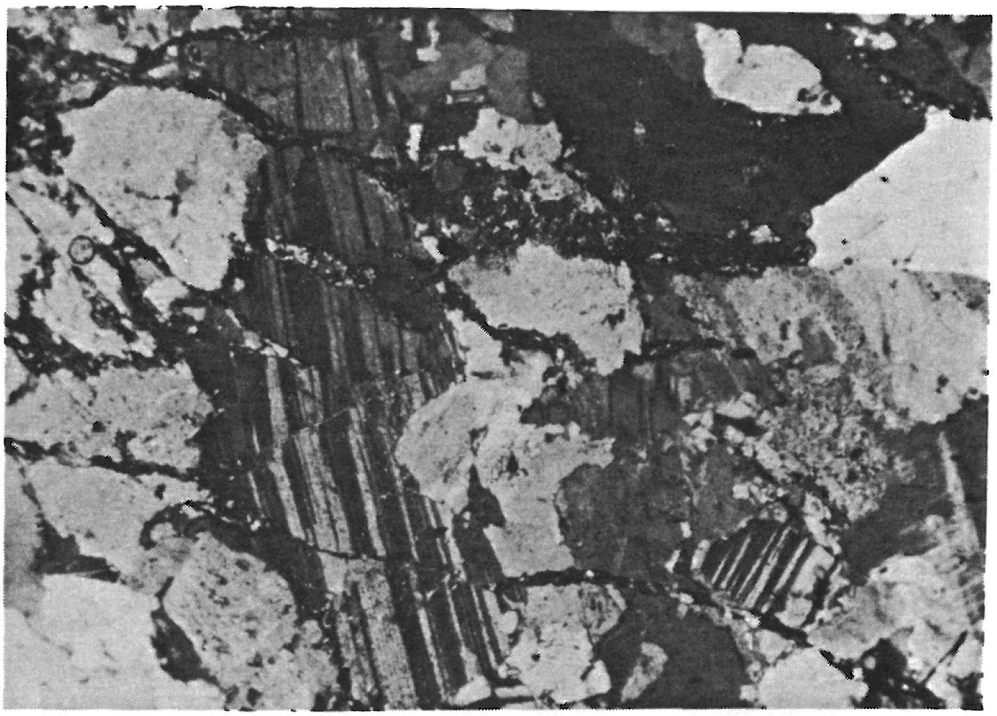

Figure 4.11 Subparallel fractures dislocating grain and grain boundaries. Area of the picture is 1.9 x 2.6 mm. Crossed Nicols.

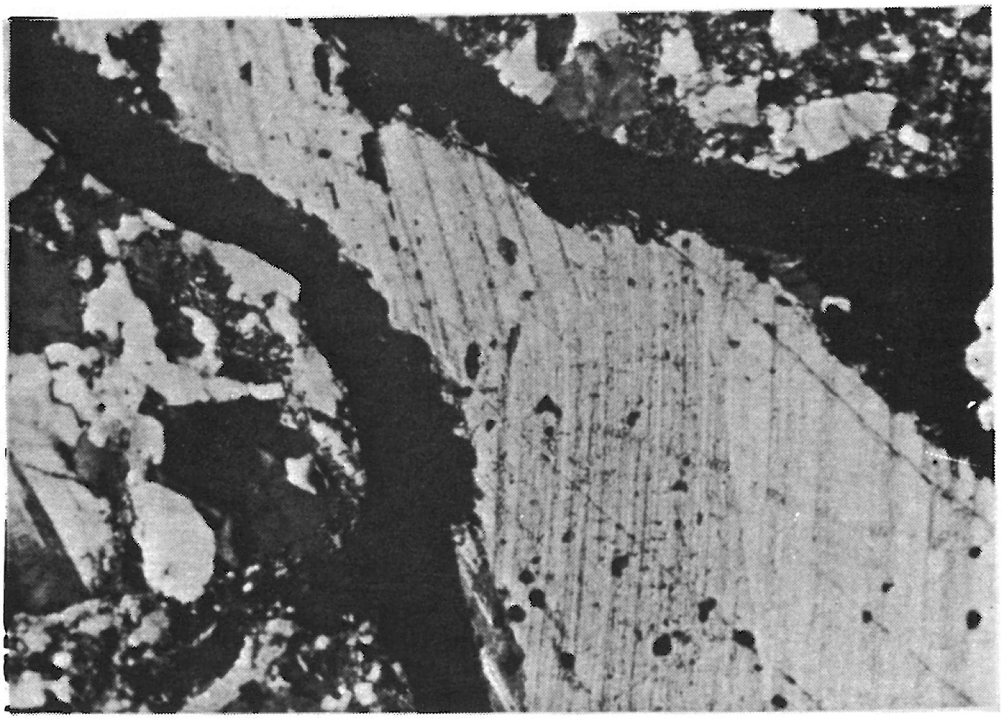

Figure 4.12 Fracture sealed by large calcite grains in its central parts and fluorite in the margins. Area of the picture is 1.9 x 2.6 mm. Crossed Nicols.

4.5 Variations of the properties within unit C.

The denser sampling across unit C in borehole F2 (1.5 samples/m) provides a good picture of the variation of physical properties across the unit. The major units are characterized by a pattern of complex and varying degrees of tectonization. This sampling profile will exemplify the variation in physical properties across the units.

Immediately in front of unit C in borehole F2 occurs unit B (111-113 m) which is a porous unit characterized by numerous cavities. Circulation of liquids in these voids have caused rather intense alteration of the unit. The unit is red coloured, intensely fractured and contains one fracture with clay minerals.

The part (113-119 m) of unit C adjacent to unit B is slightly tectonized which is evident by red colouring of the rock mass. This part has a rather low frequency of coated fractures, but a high frequency of sealed fractures. In this part a breccia (116.0-116.7 m) occurs which is evident by a network of sealed fractures.

The remaining part of unit C (119-126 m) is also red coloured and has a high frequency of both coated and healed fractures. It is intensely altered at a crushed zone (121.0-121.2 m). It contains a breccia (119.4-119.5 m) which has a similar character to the previously mentioned breccia (116.0-116.7 m). Clay mineral coating has been observed in one fracture.

Indications of weak tectonization also occurs in the section below unit C (126-137 m) which is indicated by occurrence of parts with slight red colouring.

The resistivity measured on the samples and the previously logged resistance measured by single point resistance tool, exhibit a very similar pattern across unit B and C. In this case the variation in resistivity correlates rather well with the variations in frequency of coated fractures (Figure 4.13). The fractured unit B and the fractured part of unit C are characterized by low resistivity. The part of unit C containing a high frequency of sealed fractures differ from the rest of the unit by its rather high resistivity. The weakly tectonized part below unit C has a rather high resistivity.

The measured porosity of the samples exhibit a pattern of the variation across unit B and C, which is very similar to the resistivity pattern (Figure 4.14).

In general there is an agreement between the intensity of deformation and the physical properties both on samples and in situ. The more intensely deformed sections are also the most porous and low resistive parts of the borehole.

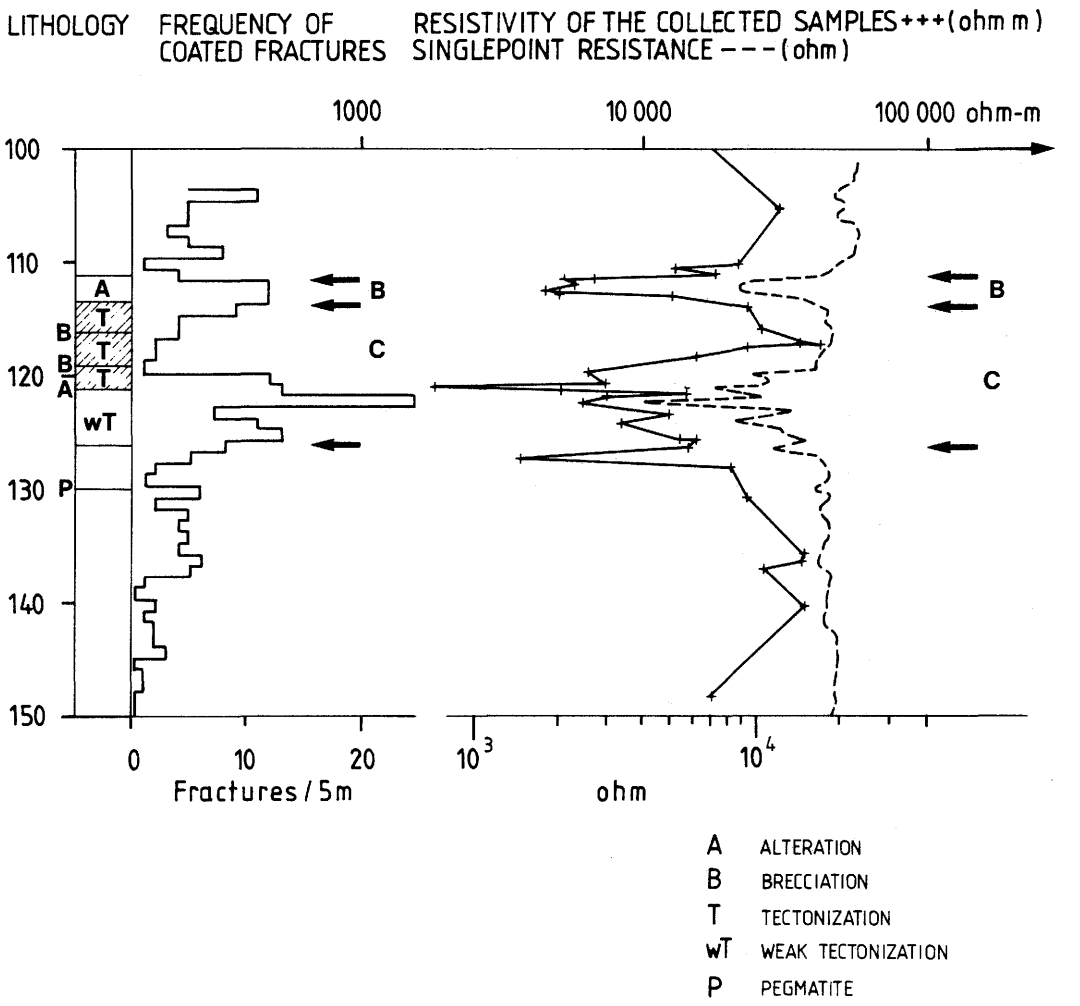

Figure 4.13 The schematic lithology, frequency of coated fractures, resistivity of the collected samples (measured at the laboratory of SGAB) and the in situ measured contact resistance (single-point resistance across unit B and C in borehole F2.

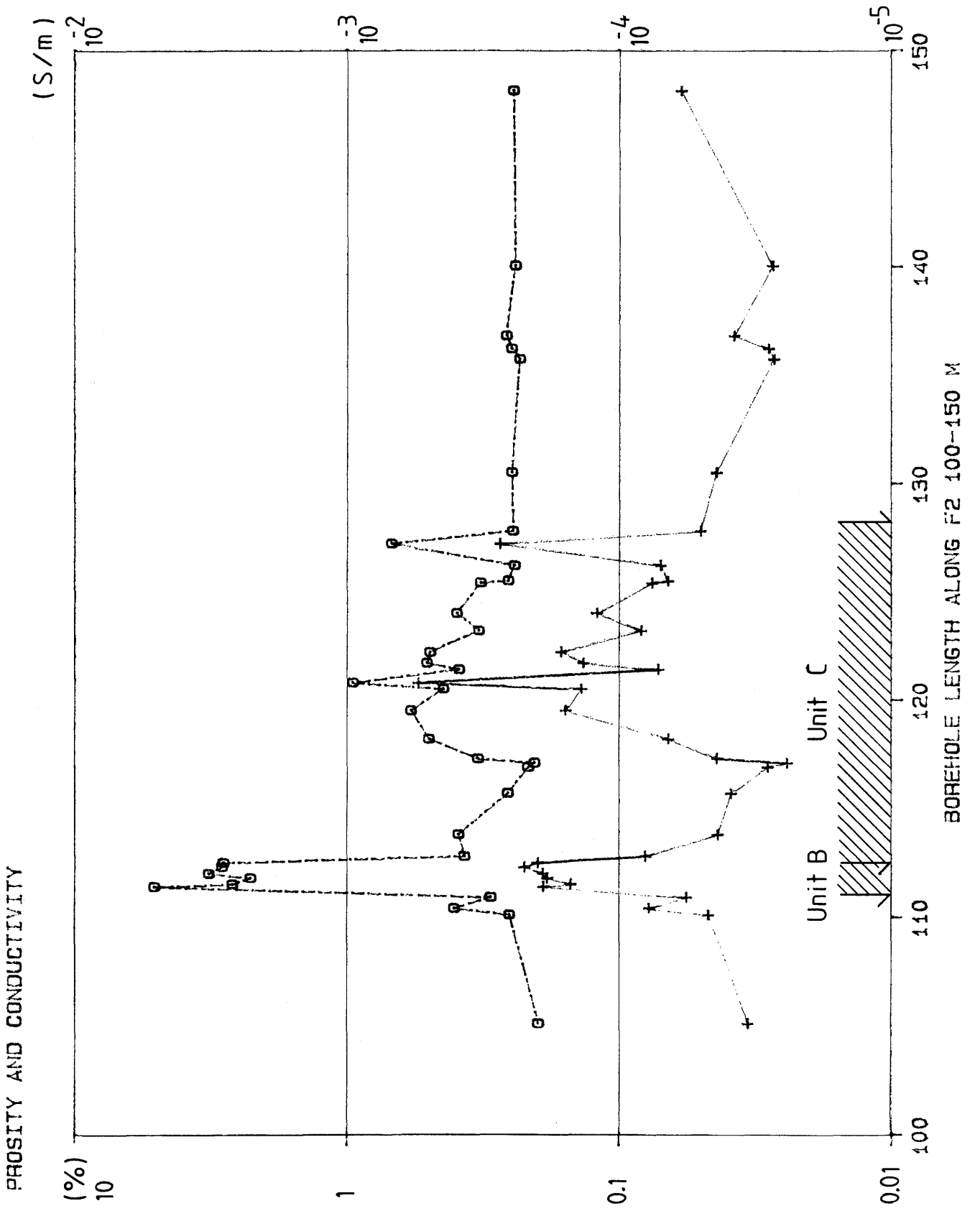

Figure 4.14 Measured immersion porosity (⊡) and the resistivity (+) of all samples collected across unit B and C in borehole F2, measured at the laboratory of SGAB.

5. HIGH FREQUENCY MEASUREMENTS OF ELECTRICAL PROPERTIES

5.1 Measurement technique

The high frequency measurements on the core samples were carried out at the Department of Applied Geophysics at the Technical University of Luleå, Sweden. These measurements were made with a Hewlett-Packard Q-meter. A description of the function and accuracy of the Q-meter has been presented by Sherman (1983).

The Q-meter measures the electrical conductance and the dielectric constant of the samples by using an LC-tank circuit which is brought into resonance by varying a capacitance in the circuit. The sample is placed in parallel to the variable circuit capacitator. The variable capacitator is then adjusted until it is in resonance and the difference in capacitance of the variable capacitator when the sample is present and when it is absent is recorded.

Both the conductance and the dielectric constant of each sample were measured at 11 different frequencies: 0.025, 0.05, 0.1, 0.2, 0.5, 1, 5, 10, 20, 50 and 70 MHz. These two physical properties were measured on each sample, both when they had been dried in an oven and after that they had been soaked in tap-water with a resistivity of approximately 40 ohm-m. The procedure of drying and soaking of the samples is described in Chapter 4.1.

The results from the high frequency measurements have recently been presented in a graduation work performed at the Technical University of Luleå (Agmalm, 1985).

5.2 Results

The results give information about the electrical conductance and the dielectrical constant of the Stripa granite at different frequencies of the applied electric field.

The major units have higher average porosity, electrical conductance and dielectric constant than the more undeformed granite. The logarithmic average values of the conductance and dielectric constant for the 11 measured frequencies have been calculated separately for all samples from the major units and the more undeformed granite. These logarithmic mean values of the conductance and dielectric constant for the eleven different frequences have been plotted in log-log scale and

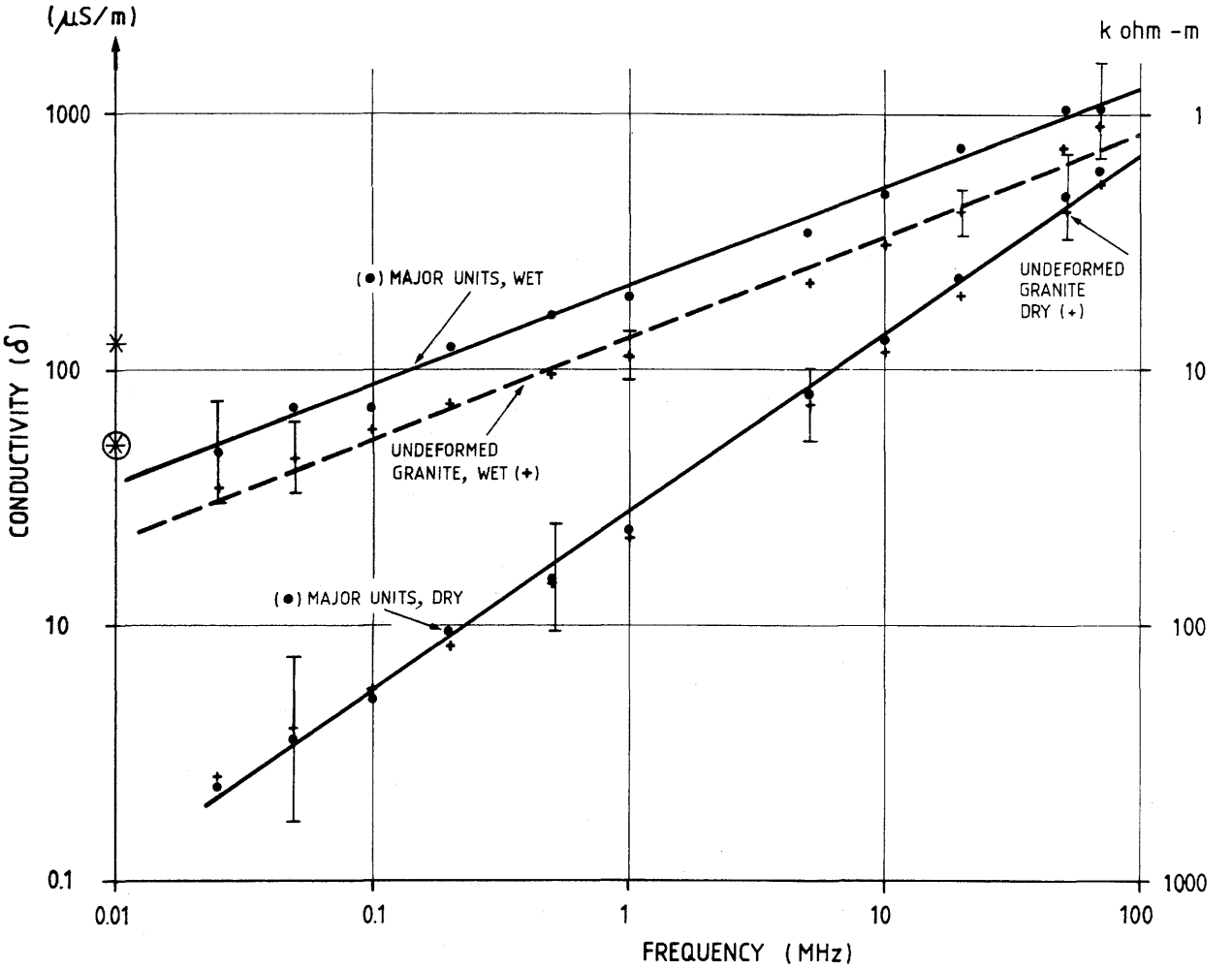

Figure 5.1 The relation between the conductivity of the samples and the frequency of the applied electric field, measured at the laboratory of the Technical University of Luleå. The average conductivity measured at low frequencies at the laboratory of SGAB, for major units (*) and undeformed granite (⊛).

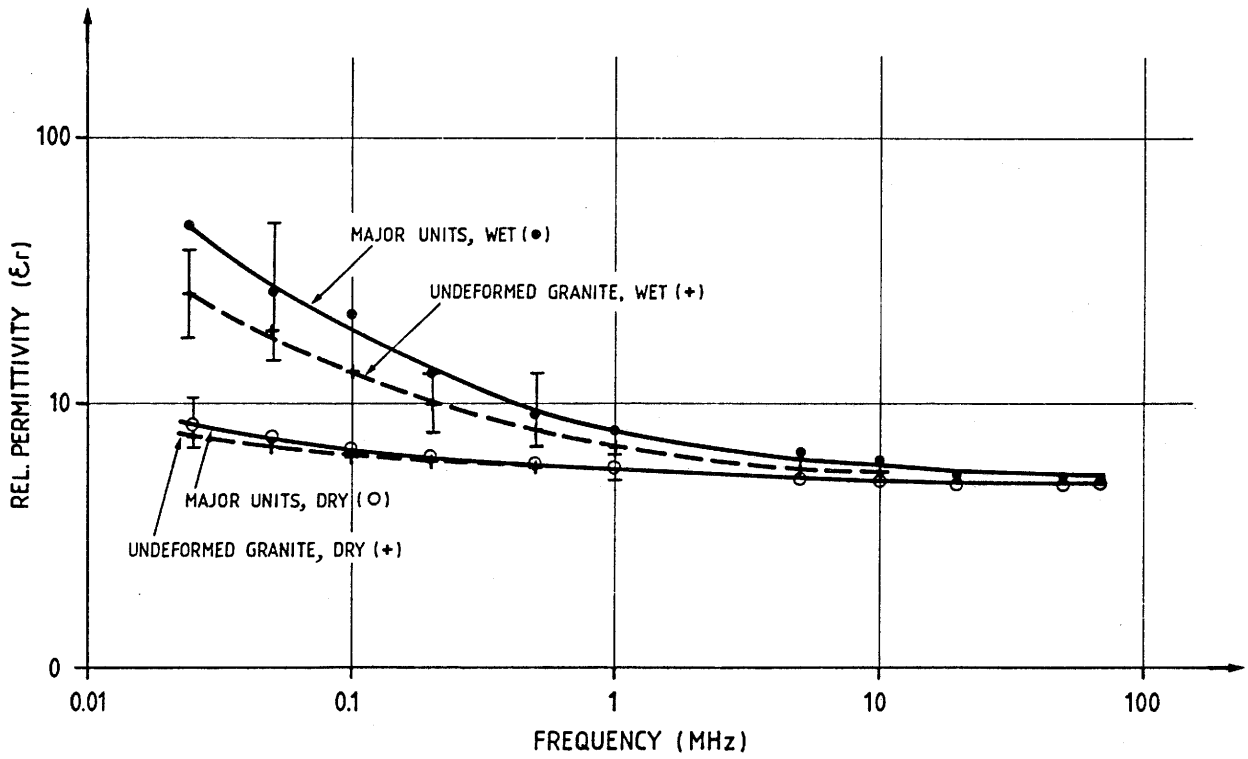

Figure 5.2 The relation between the dielectric constant of the samples and the applied electric field, measured at the laboratory of the Technical University of Luleå.

presented in Figures 5.1 and 5.2. The properties for both dry and soaked samples are presented in these figures.

The soaked samples have considerably higher conductance and dielectric constant at lower frequencies than the dry rock samples. But at higher frequencies the difference in conductivity is much smaller and the difference in dielectric constant very small. The wet samples from the major units have markedly higher conductance and dielectrical constant than the wet samples from the undeformed granite, while the dry samples from the major units and the undeformed granite exhibit a very small difference in dielectric constant and no difference in conductivity.

In the log-log plot of the coductivity vs. the frequency, the conductivity of the wet samples exhibit an almost linear increase in conductivity with increasing frequency. The samples from the major units have a higher average conductivity than the samples from the undeformed granite but the same linear increase with the frequency, i.e. both of them increase with the exponent 0.38 of the frequency. The dry samples also exhibit linear increase in log-log scale, but no significant difference in conductivity between the undeformed granite and the major unit. The conductivety of the dry samples increases with the exponent 0.68 of the frequency (Figure 5.1).

The dielectric constant of the wet samples decreases markedly with increasing frequency from values about 50 (major unit) or 30 (undeformed granite) to low values of about 5 after 5 MHz. The dry samples have a much lower dielectric constant which also decreases with increasing frequency from about 8 to about 5 after 5 MHz (Figure 5.2).

5.3 Comparison between high and low frequency measurements of the resistivity.

The measurement of the resistivity at low frequency (1 Hz) results in lower average values of the resistivity than the measurements at 25 kHz. The low frequency measurements were carried out at the SGAB laboratory and the high frequency measurement at the Technical University of Luleå. Note, that the sizes of the samples were decreased before the high frequency measurements and that the average porosity changed after changing the size, see Chapter 4.1. However, the log-log linear decrease in resistivity with increasing frequency of the applied electric field is expected to result in a considerably higher resistivity at 1 Hz compared to 25 kHz. From Figure 5.1 it is evident that the

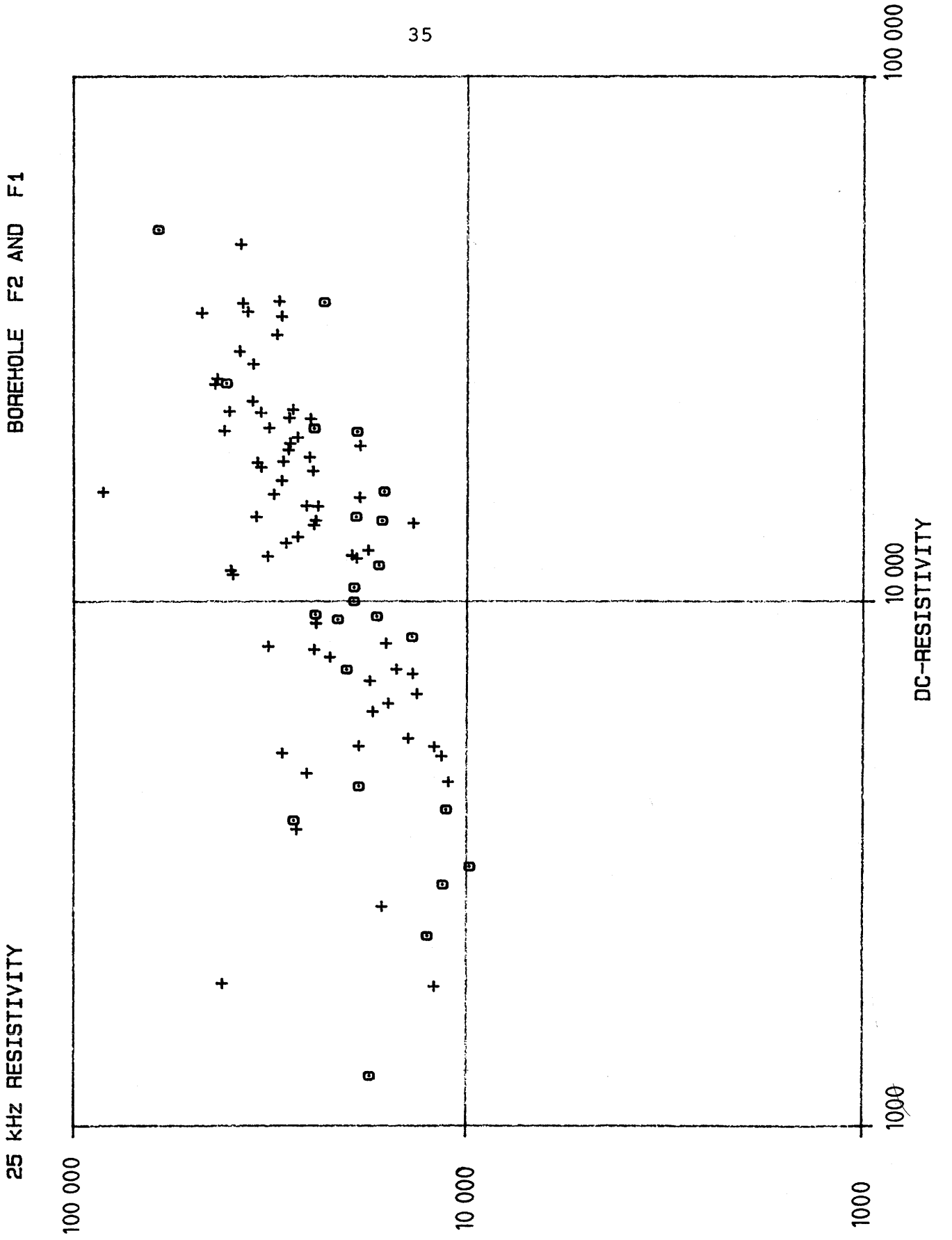

Figure 5.3 Cross-plot of the resistivity measured at low frequencies (1 Hz) at the laboratory of SGAB vs resistivity measured at 25 kHz at the laboratory of the Technical University of Luleå.

resistivity will continue to increase also at frequencies lower than 25 kHz.

The cross-plot of low frequency measurements (1 Hz) and high frequency mesurements (25 kHz) exhibits a rather large scattering (Figure 5.3). This may to a large extent be an effect of the fact that the physical properties have changed considerably after the sample size was decreased.

The in situ measurements (1 Hz) of the resistivity result in a considerably higher average resistivity compared to the low frequency measurements on the samples carried out at the SGAB laboratory in Malå. For example the undeformed granite generally has values higher than 100 kohm-m (Carlsten et. al., 1985). The in situ measurements will also be influenced by fractures, while the current transport through the rock samples takes place through the microscopic and hairline fractures. The contribution of current transport through the fractures is therefore expected to result in lower in situ resistivities.

Both the high frequency measurements and the in situ measurements indicate that the low frequency measurements result in too low values for the resistivity. The low frequency measurements are therefore probably influenced by leakage of current along the surface of the samples. It should be kept in mind that the measurements are rather sensitive to the dampness of soaked sample surfaces as shown by Öquist (1981).

6. CORRELATION OF INVESTIGATED PROPERTIES

6.1 Correlation between porosity and resistivity

The measured resistivity at the low frequency (1 Hz) and the immersion porosity measured at SGAB laboratory in Malå exhibit a similar pattern of variation along the borehole. This is demonstrated in Figures 4.4 and 4.5, which show the variation of porosity and conductivity (1/resistivity) along boreholes F1 and F2. The undeformed granite between the major units is characterized by more uniform low porosity and high resistivity, while the major units generally have higher porosity and lower resistivity.

The crossplot in log-log scale of porosity vs resistivity of the samples from the undeformed rock mass between the major units in F1 and F2 is clustered in the high resistivity (mean value 20 000 ohmm) and low porosity (mean value 0.25 %) region (Figure 6.1).

The crossplot in log-log scale of porosity vs resistivity of the samples from the major units exhibits a more or less linear relationship between porosity and resistivity, where the resistivity decreases with increasing porosity (Figure 6.2). This is in agreement with the empirical law found by Archie (1942). This relation is not evident in the crossplot of samples from the undeformed rock.

In clean saturated mixtures of non-conductive rock matrix and conductive electrolyte Archie's law describes the relation between resistivity and porosity as follows:

$$F = R/R_w = a\,\phi^{-m}$$

F = formation factor
R = formation resistivity
R_w = water resistivity
ϕ = porosity
a : for saline solutions Archie found that a is approximately 1.
m : for saline solutions Archie found that m varies between 1.8 and 2.

Archie's law was established from measurements on samples from sedimentary rocks. Brace et. al., (1965) have found that Archie's law also holds for igneous rocks and the exponent m was then approximately 2. However, other measurements on igneous rocks by Brace and Orange (1968) have demonstrated that the exponent m can vary between 1 and 2. A theoretical study by Sen et. al., (1981)

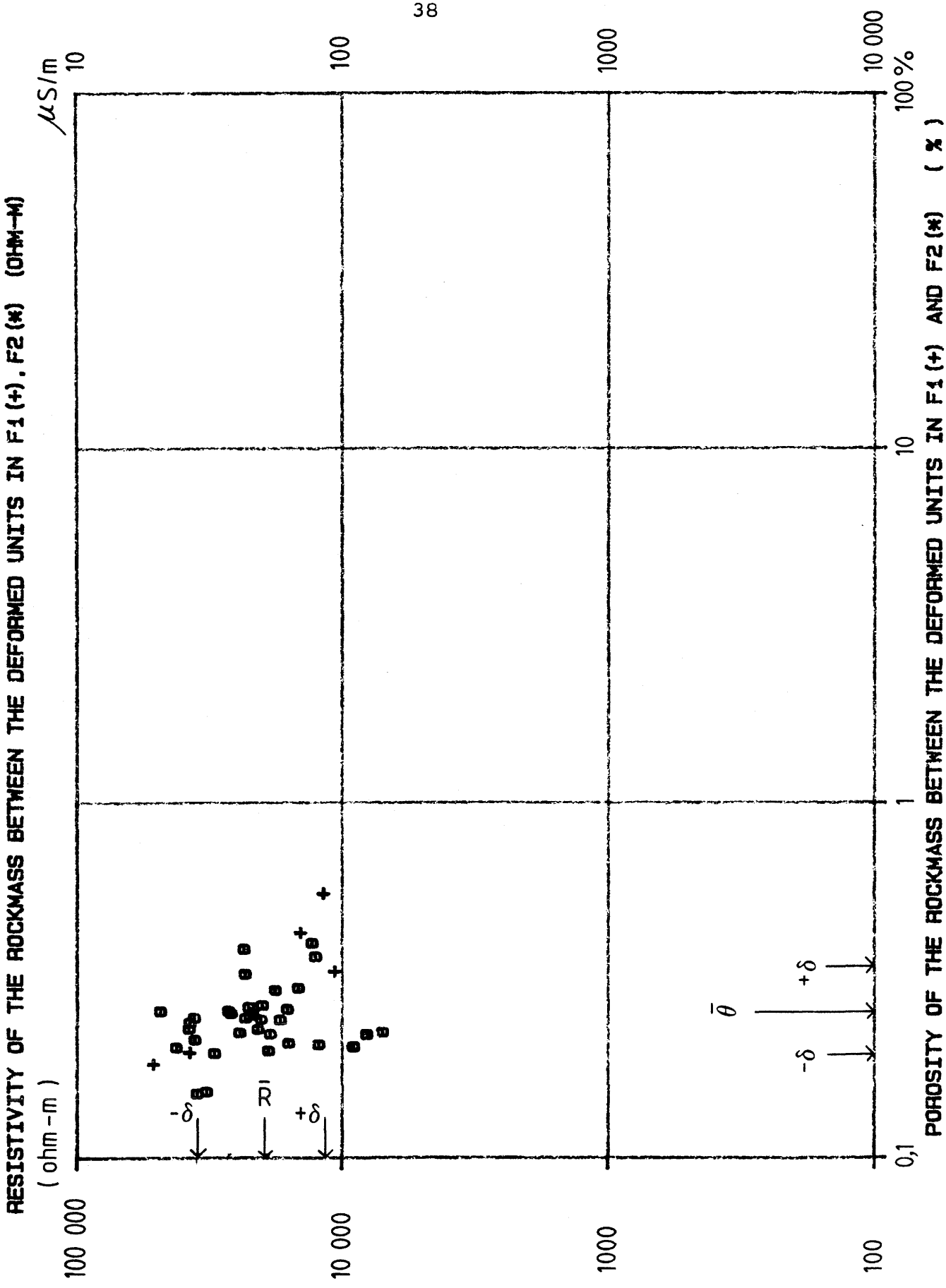

Figure 6.1 The measured immersion porosity vs the resistivity of samples from the more undeformed granite, log-log scale. Measured at the laboratory of SGAB.

assuming that nonconducting rock particles are dispersed in a continuous phase of pore-water shows that the exponent m for spherically shaped particles is 3/2, for needle-shaped the exponent is m=1 and for plate-like shapes the exponent m can be considerably larger than 3/2.

In igneous compact rocks with very low porosity, less than 1 %, Archie's law, which is a log-log linear relation between resistivity and porosity, is invalid for pore water resistivities above 20 ohmm (Brace et. al., 1965 ; Öquist, 1981). The reason for this is that the so called surface conduction along thin water films and pore grain interfaces will be several times greater than the volume conduction by ions through the pore spaces. According to Brace et. al., (1965) and Nelson et. al., (1982), Archie's law can be rewritten by adding a surface conductive element in parallel with the volume conduction in the pore-water.

In 1968 Waxman and Smith proposed the first extensive model of shaly sand formations where clay particles contribute exchange cations with the electrolyte and thereby increase the conductivity. They considered that the electrical conductance of shaly sand formations can be represented by two resistive elements in parallel, which is in agreement with the statement above, i.e. the electrical surface conduction contributes to the conductivity in a similar manner as the clay particles in the shaly sand formations.

$$1/R = 1/R_s + (1/R_w)\phi^{-m}$$

$1/R_s$ = electrical surface conductivity

The rewritten formula can also be presented in the following form:

$$C - C_s = C_w \phi^m$$

$$\log (C - C_s) = m \log \phi + \log C_w$$

C = formation conductivity
C_s = surface conductivity
C_w = water conductivity

The different contributions from surface conduction (C_s) have been tested by assuming different values of the surface conduction. The assumed value of surface conduction is subtracted from the measured conductance and thereafter the logarithm of the difference is calculated and plotted against the logarithm of the measured porosity. Thereafter, the relation of the porosity is calculated by linear regression, the slope corresponds to the

exponent m. The results from a series of such tests are shown in Table 6.1.

Table 6.1 Tested values of surface conduction.

C_s (S/m)	m	Corr.coeff.
0	-1.1	-0.74
0.01	-1.2	-0.74
0.02	-1.3	-0.73
0.03	-1.5	-0.72
0.035	-1.7	-0.67

As can be seen from Table 6.1 the assumed value 0.03 for the surface conduction gives a value of the exponent m which is in agreement with the theoretical study of Sen et. al. (1981), for spherical shapes of the particles. Brace et. al. (1965) found from measurements on samples from igneous rocks that the exponent m is often close to 2. However, for larger values of surface conduction than 0.3 the correlation coefficient will be rather small. We therefore assume that values of surface conduction of about 0.03 will be the best estimate of the surface conduction.

The major unit B characterized by numerous cavities is an extremely porous granite and exhibits a different relation between the porosity and resistivity than the other samples (Figure 6.2). Although unit B has a porosity several times that of other fractured units it is not the zone of lowest resistivity. Neither do the samples from this unit contain the most low resistive samples (Figures 4.4 and 4.5). This unit has a porosity of vuggy character, with a large number of the pores that are not electrically well connected. The different pore geometry results in a different cementation factor, i.e. a different exponent in Archie's formula.

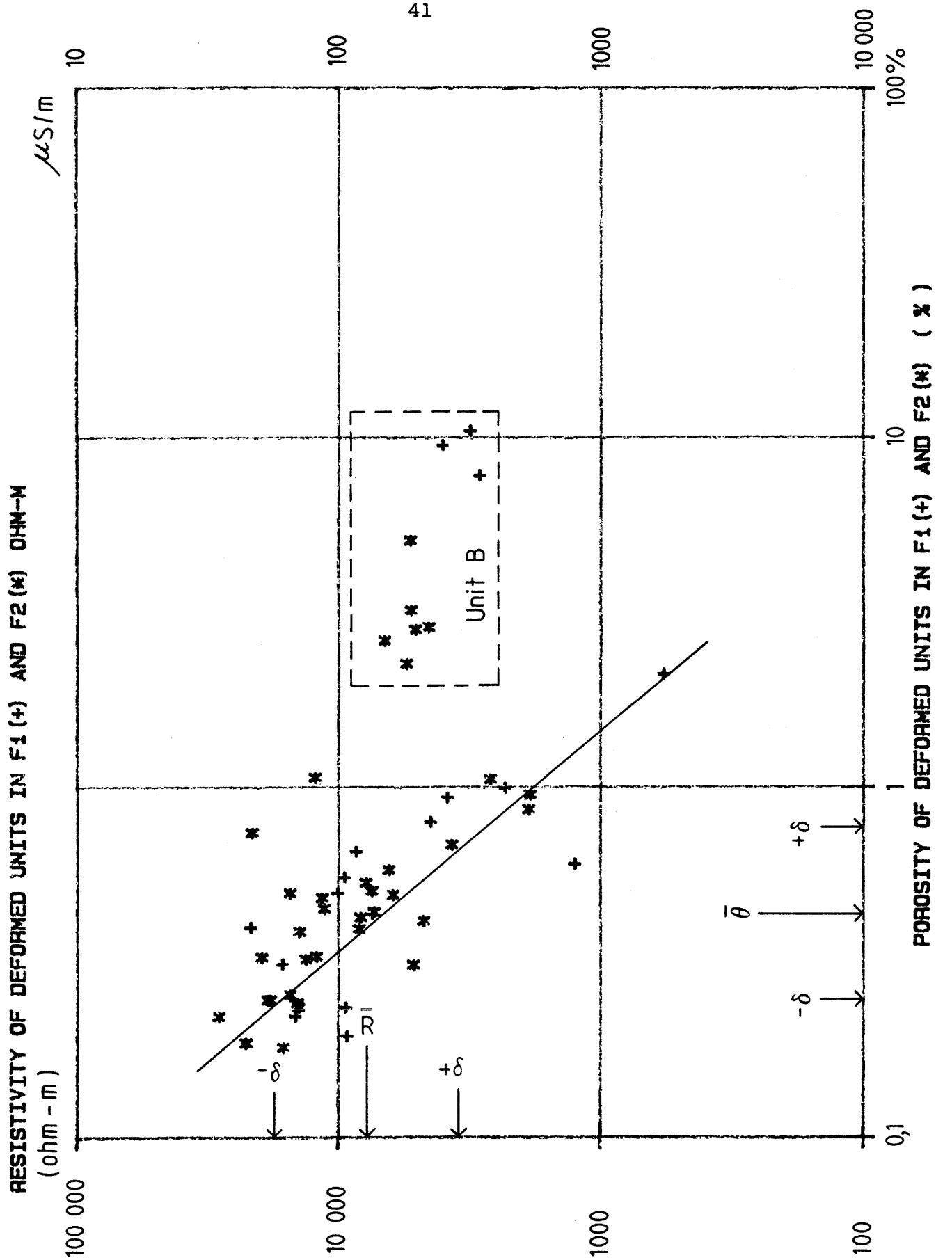

Figure 6.2 The measured immersion porosity vs the resistivity of samples from the major units, log-log scale. Measured at the laboratory of SGAB.

6.2 Porosity predictions by Hanai-Bruggeman formula

The dielectric constant of a heterogeneous medium such as saturated rocks depends on the pore fluid, the porosity, the matrix and the frequency of the applied electric field.

The Hanai-Bruggeman equation relates the effective dielectric constants of a heterogeneous material to the volume fraction of its constituents. In Maxwell's equations the conductivity and dielectric constant occur as a combination in form of a complex effective dielectric constant:

$$\varepsilon^* = \varepsilon' + i\varepsilon'' = \varepsilon + i\ (\sigma/\omega)$$

σ = conductivity
ε = dielectric constant
ω = angular frequency

The Hanai-Bruggeman equation describes the electric bulk behaviour of a heterogeneous mixture of constituents with different electrical properties. The theoretical study by Sen et. al., (1981) has shown that the Hanai-Bruggeman equation can be deduced by assuming that nonconducting rock particles are dispersed in a continuous phase of pore-water, i.e. the rock constitutes an assembly of water-coated grains. The Hanai-Bruggeman equation is :

$$\left(\frac{\varepsilon^* - \varepsilon^*_m}{\varepsilon^*_w - \varepsilon^*_m}\right)\left(\frac{\varepsilon^*_w}{\varepsilon^*}\right)^L = \phi$$

ε^* = The bulk complex dielectric constant of the water saturated rock.
ε^*_m = The complex dielectric constant of the rock matrix.
ε^*_w = The complex dielectric constant of water.
ϕ = The porosity of the rock.
L = The depolarization factor.

The exponent called the depolarization factor is considered to be independent of the frequency of the applied electric field. Sen et. al., (1981) has shown that the depolarization factor depends on the shape of the dispersed nonconducting rock particles.

L = 1/3 for spheres.
L = 0 for needles with axis parallel to the field.
L = 1/2 for cylinders with their axis perpendicular to field.

Sen et. al. (1981) have shown that when the frequency of the electric field approaches zero,

the depolarization factor is related to the cementation exponent in Archie's equation.

In this investigation the measurements on dry samples are considered to represent the electric properties of the matrix, while measurements on soaked samples represent the bulk electric properties of the water saturated rock.

The effect of the complex dielectric constant of the pore water was tested by assuming different values of relative dielectric constant and the electric conductivity. The porosity was then calculated for different frequencies according to Hanai-Bruggeman equation using the measurements for both dry and water saturated samples. It should be noted that the Hanai-Bruggeman equation uses complex input parameters to calculate the porosity which is a real valued quantity. Thus, a good check on the consistency of the data introduced into the equation is that the calculated porosity should be real. This has been the main criteria in the determination of realistic values for parameters which can not be measured directly. The calculations show that the relative dielectric constant can be considered to depart very little from the value 81 of water. Even if the assumed values of the dielectric constant depart considerably from 81, the calculated porosity differs very little (Figures 6.3 and 6.4). Thus, the assumed value of 81 can be used as a good estimate in a calculation of the porosity. The exponent 0.333 and the pore water resistivity 40 ohm-m were used in the calculated porosities presented in Figures 6.3 and 6.4.

Values for the conductivity between 0.1-0.025 S/m resulted in a very small imaginary component of the calculated porosity and porosity values calculated with Hanai-Bruggeman equation similar to those measured at different frequencies on the core samples (Figures 6.5 and 6.6). The samples were soaked with tap water which has a conductivity about 0.025 S/m (resistivity = 40 ohm-m). However, the formation water conductivity is probably around 0.1 S/m (resistivity = 10 ohm-m) due to the fact that some pore-water and salt is probably left after the drying procedure of the samples. The average pore water conductivity is thus probably somewhat higher than 0.025 S/m. This is then in agreement with the values which give the best estimate of the calculated porosity. Thus, the values between 0.025-0.1 S/m can be considered as good estimates of the average conductivity of the pore water. The exponent 0.333 and a dielectric constant of 81 for the pore water were used in the calculations of the porosity presented in Figures 6.5 and 6.6.

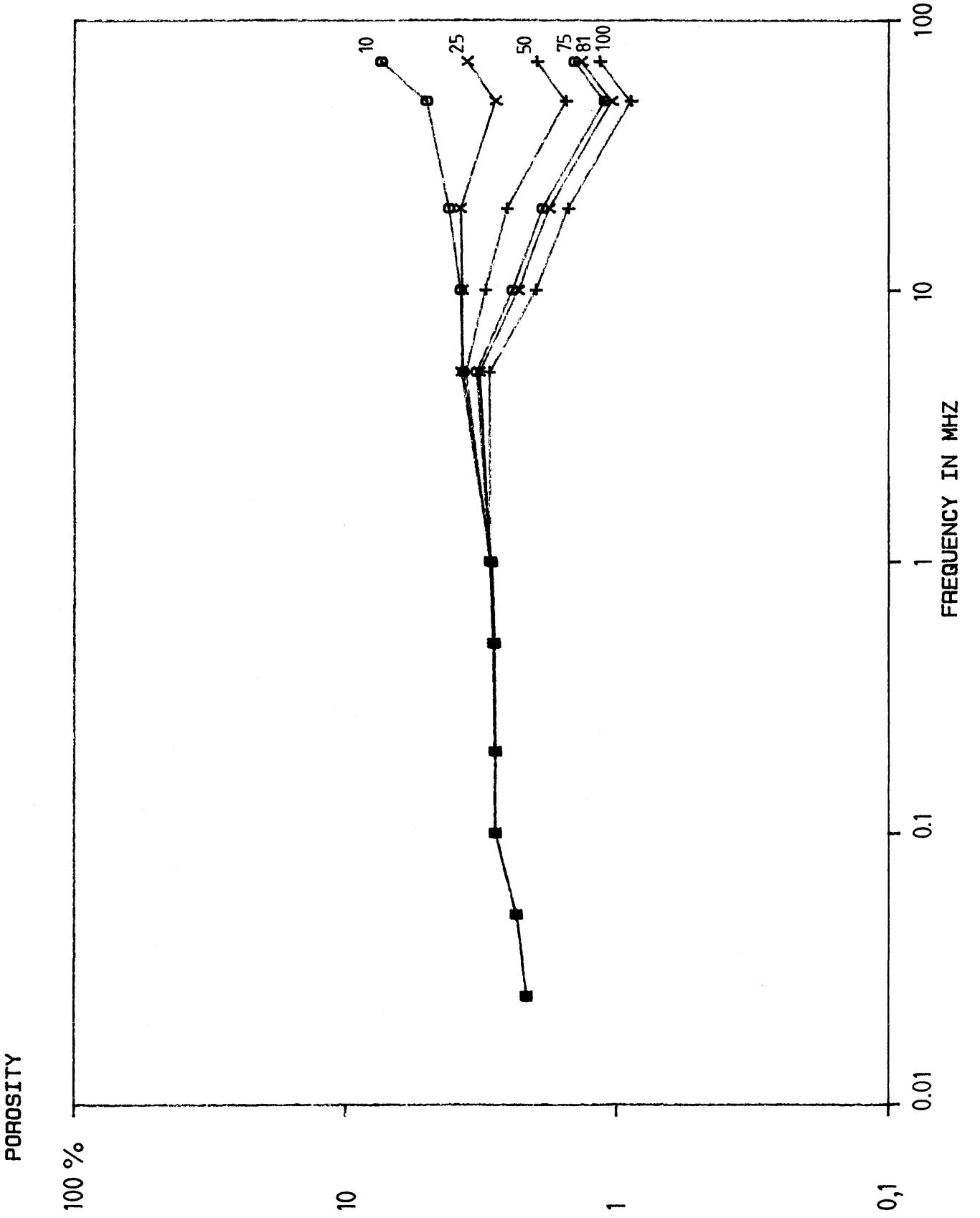

Figure 6.3 Porosity (real component) of one selected sample calculated by the Hanai-Bruggeman equation for different assumed values of the relative dielectric constant of the pore-water: 10, 25, 50, 75, 81 and 100. The assumed value of the depolarization factor is 0.333 and the assumed value of the pore-water resistivity is 40 ohm-m.

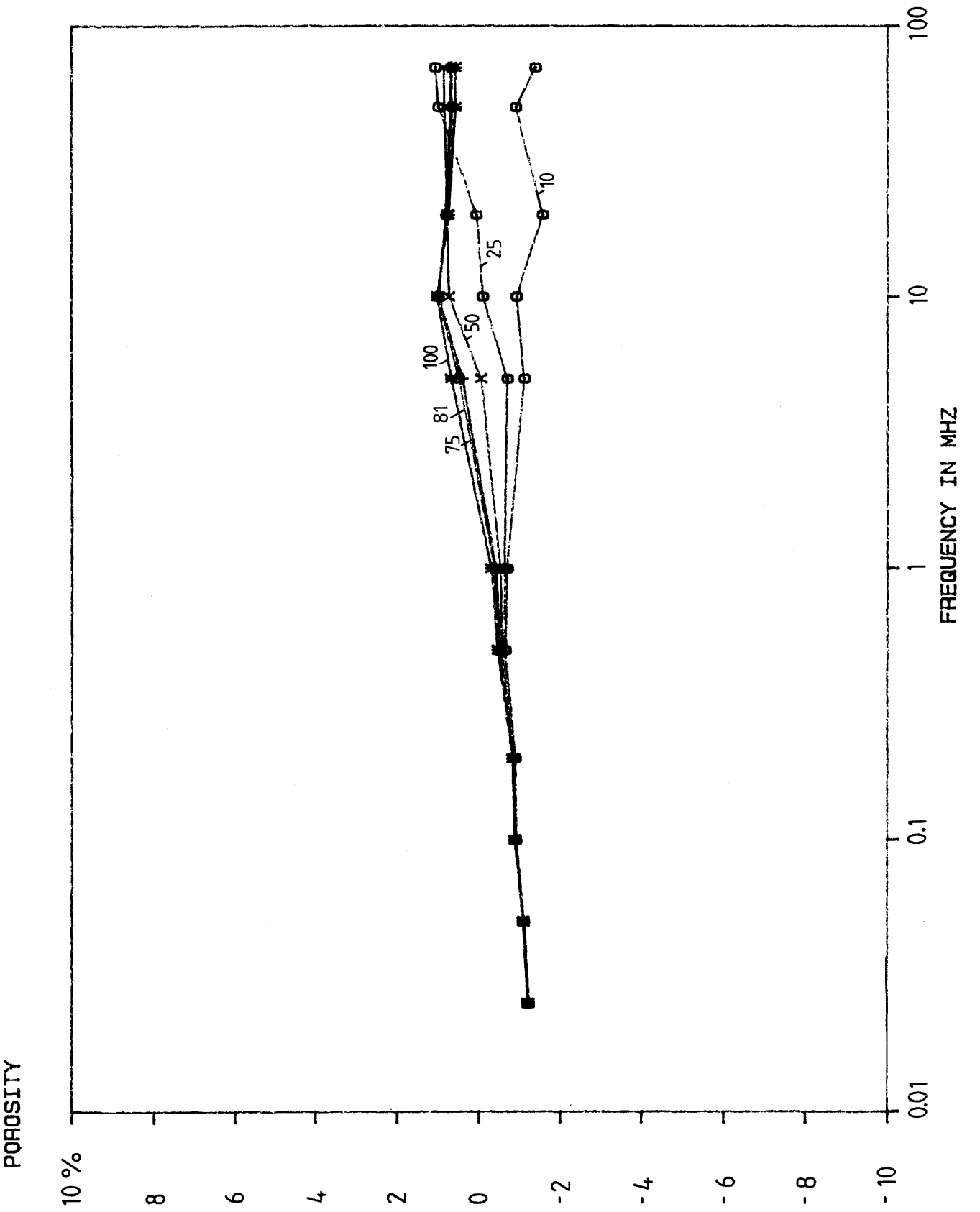

Figure 6.4 Porosity (imaginary component) of one selected sample calculated by Hanai-Bruggeman equation for different assumed values of the relative dielectric constant of the pore-water: 10, 25, 50, 75, 81 and 100. The assumed value of the depolarization factor is 0.333 and the assumed value of the pore water resistivity is 40 ohm-m.

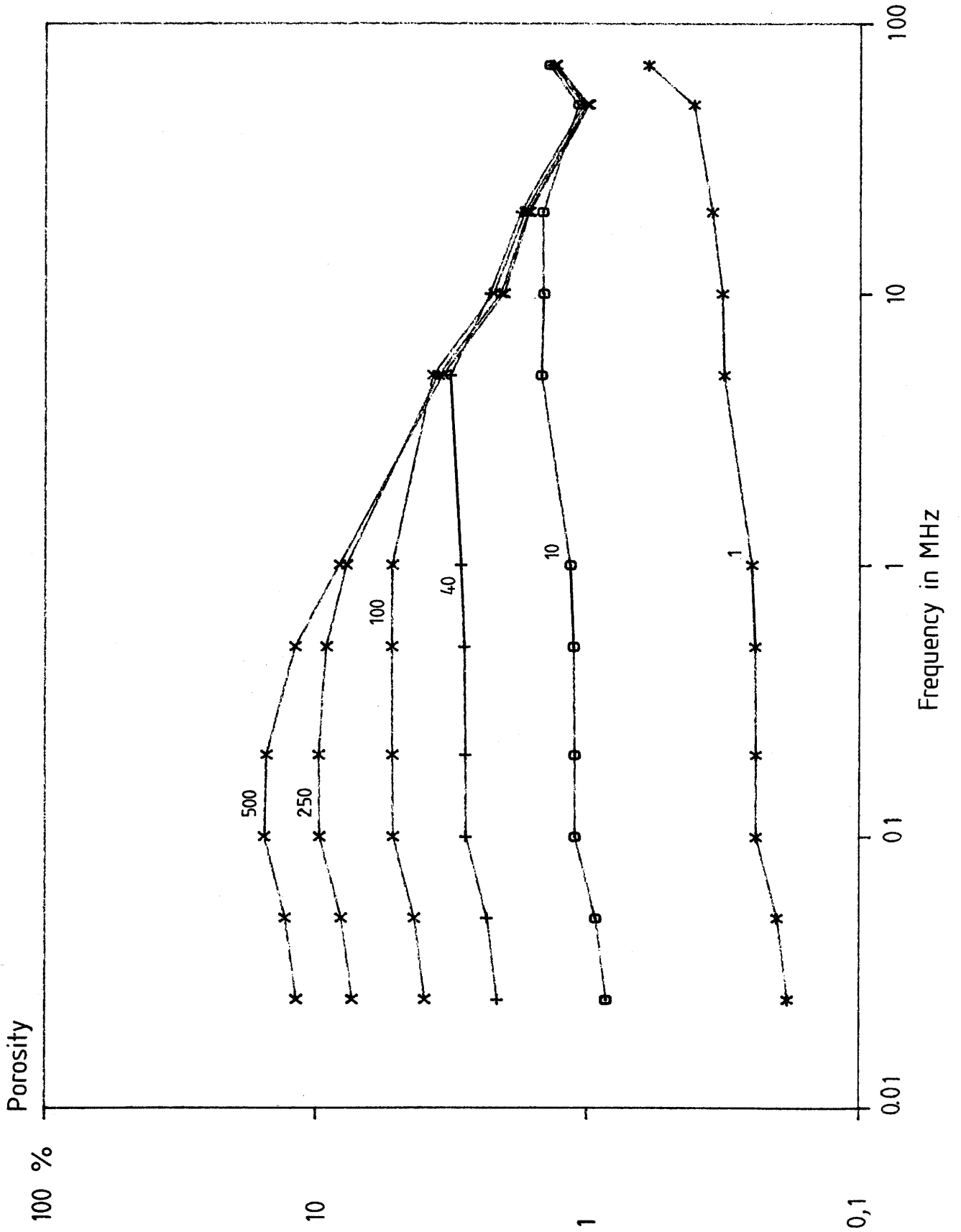

Figure 6.5 Porosity (real component) of one selected sample calculated by the Hanai-Bruggeman equation for different assumed values of the resistivity of the pore-water: 1, 10, 40, 100, 250 and 500 ohm-m. The assumed value of the depolarization factor is 0.333 and the assumed value of the pore-water dielectric constant is 81.

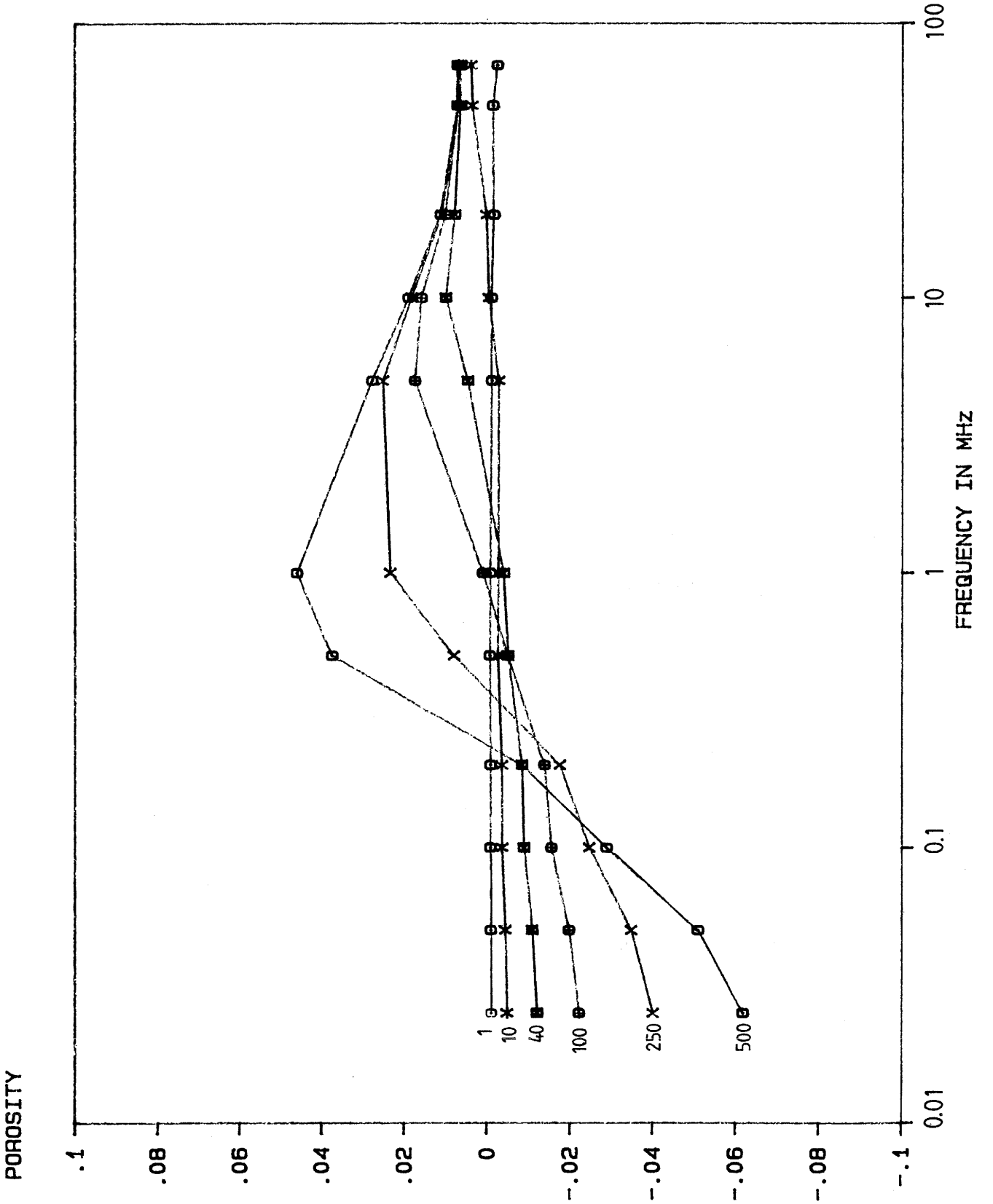

Figure 6.6 Porosity (imaginary component) of one selected sample calculated by the Hanai-Bruggeman equation for different assumed values of the resistivity of the pore-water: 1, 10, 40, 100, 250 and 500 ohm-m. The assumed value of the depolarization factor is 0.333 and the assumed value of the pore-water dielectric constant is 81.

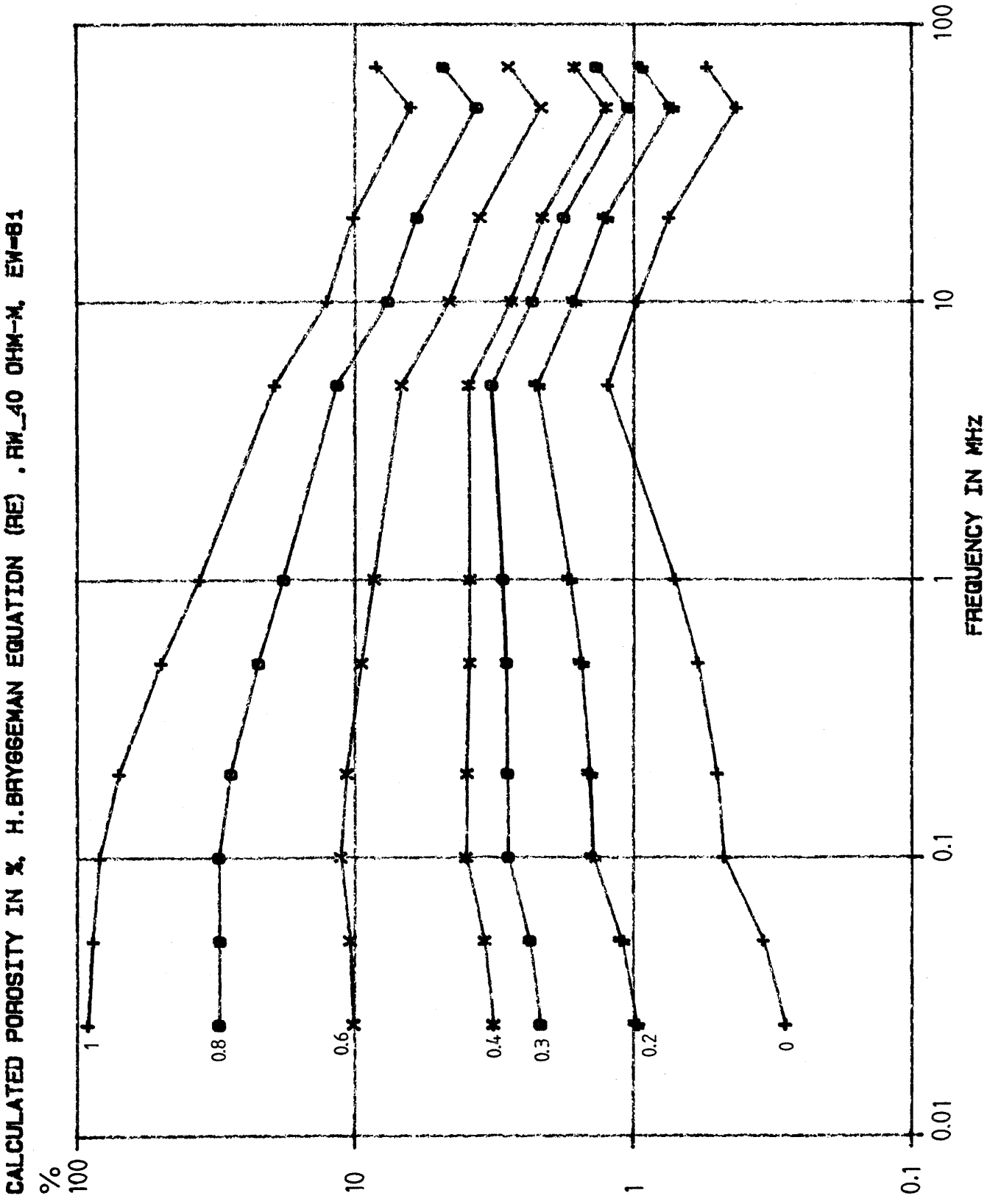

Figure 6.7 Porosity (real component) of one selected sample calculated by the Hanai-Bruggeman equation for different depolarization factors: 1, 0.8, 0.6, 0.4, 0.3, 0.2 and 0. The assumed values of resistivity and dielectric constant are 40 ohm-m and 81, respectively.

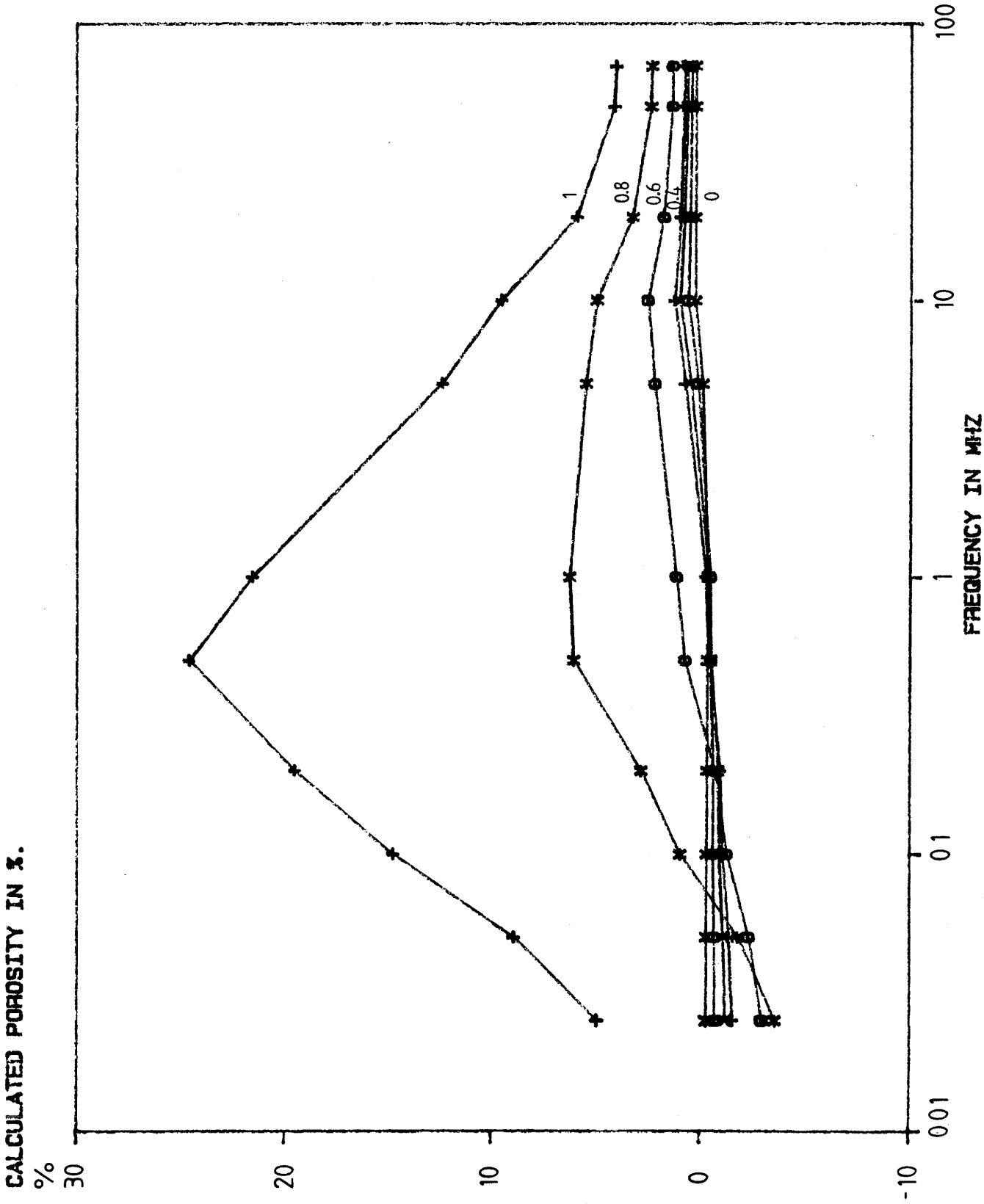

Figure 6.8 Porosity (imaginary component) of one selected sample calculated by the Hanai-Bruggeman equation for different depolarization factors: 1, 0.8, 0.6, 0.4, 0.3, 0.2 and 0. The assumed values of resistivity and dielectric constant are 40 ohm-m and 81, respectively.

Different polarization factors (the exponent in the Hanai-Bruggeman equation) have also been tested. Values of the exponent between 0-0.4 give very small imaginary components. Also, values between 0.2-0.4 give reasonable values for the calculated porosity (Figures 6.7 and 6.8). The value 1/3 will according to Sen et. al. (1981) result in an cementation factor of 3/2 Archie's equation. This is in agreement with results for low frequency measurements presented in Chapter 6.1, which show that the cementation factor is approximately 3/2. The depolarization factor 1/3 for spheres can therefore be considered to be rather close to the true factor. In the calculation of the porosity presented in Figures 6.7 and 6.8, the dielectric constant 81 and the resistivity 40 ohm-m were used for the pore water.

The porosity calculated according to Hanai-Bruggeman equation has been plotted against the measured immersion porosity, measured at the laboratory at the Technical University of Luleå. The porosity was calculated for 0.025, 1 and 20 MHz. The calculation of the porosity has been carried out with the depolarization factor 0.333 and with the following values for the dielectric constant and conductivity of the water, respectively: 81 and 0.2 S/m. Note that in analogy with the low frequency measurements the different pore geometry of unit B results in a different depolarization factor. Thus, these samples exhibit a different trend in the plot of the calculated porosity against the measured values (Figures 6.9, 6.10 and 6.11).

The calculated values for 1 and 20 MHz exhibit a better correlation (Correlation coefficients: 0.78 and 0.72) with the measured porosity than those for 0.025 MHz (Correlation coefficient: 0.63). The calculated porosity for the higher frequency gives somewhat higher values compared to the lower frequencies.

The porosity calculated by Hanai-Bruggeman equation results in a higher average value of the porosity compared to the measured immersion porosity. In the high frequency measurements the isolated pores such as the fluid inclusions also contribute to the electrical bulk properties. This type of pores are not expected to contribute to the measured immersion porosity. The fluid inclusion pores in the Stripa granite constitute 0.49 % of its rock mass according to Lindblom (1984) i.e. it is of the same order of magnitude as the immersion porosity (mean value for the major units is 0.43 %). Note, that the fluid inclusions contain saline brine pore-water with an average salinity of about 3 wt. % (Lindblom, 1984). The porosity calculated from

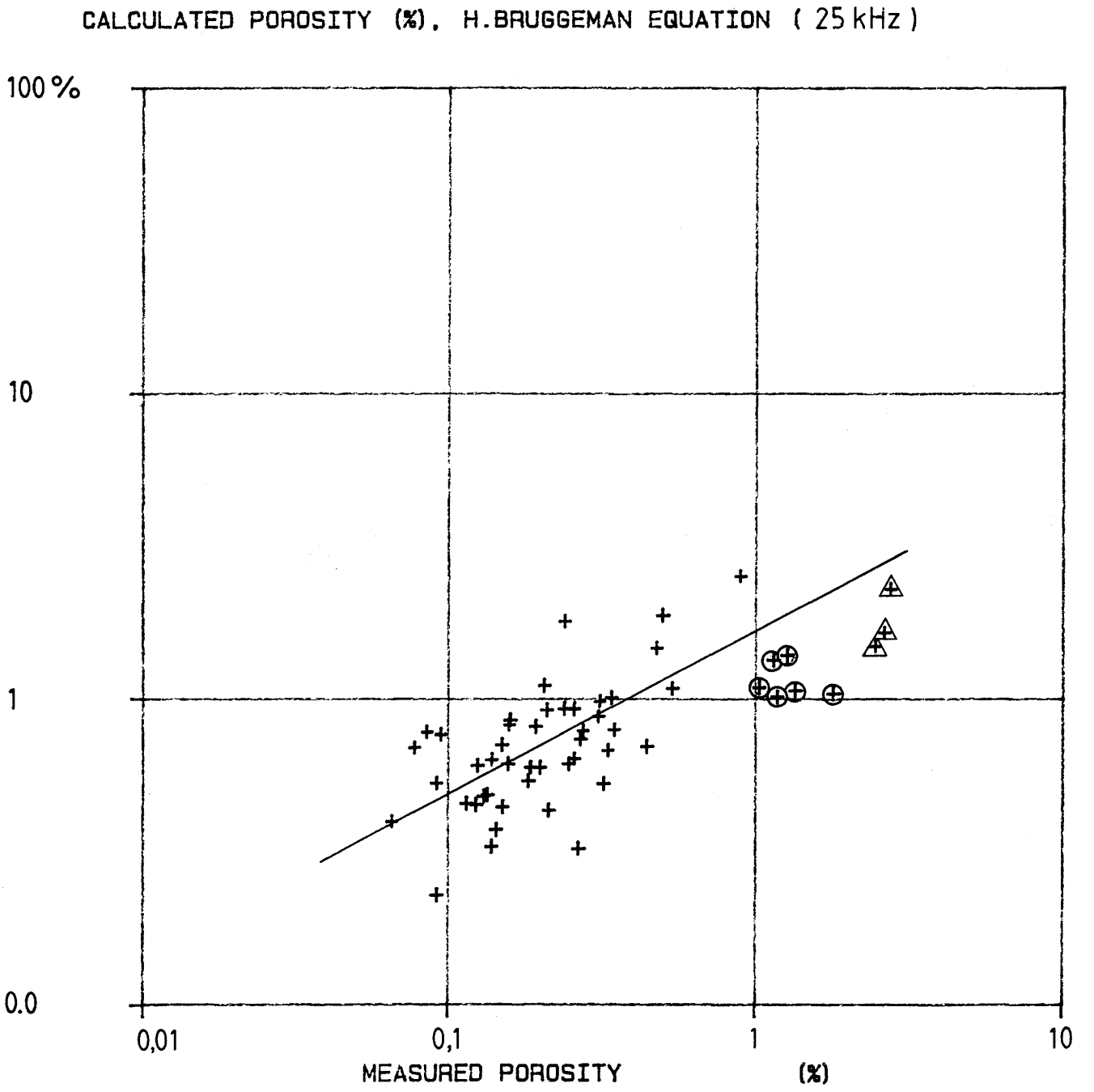

Figure 6.9 Measured immersion porosity (measured at the laboratory of the Technical University of Luleå) vs the calculated porosity according to Hanai-Bruggeman equation. All samples measured with 25 kHz frequency of the applied electric field.

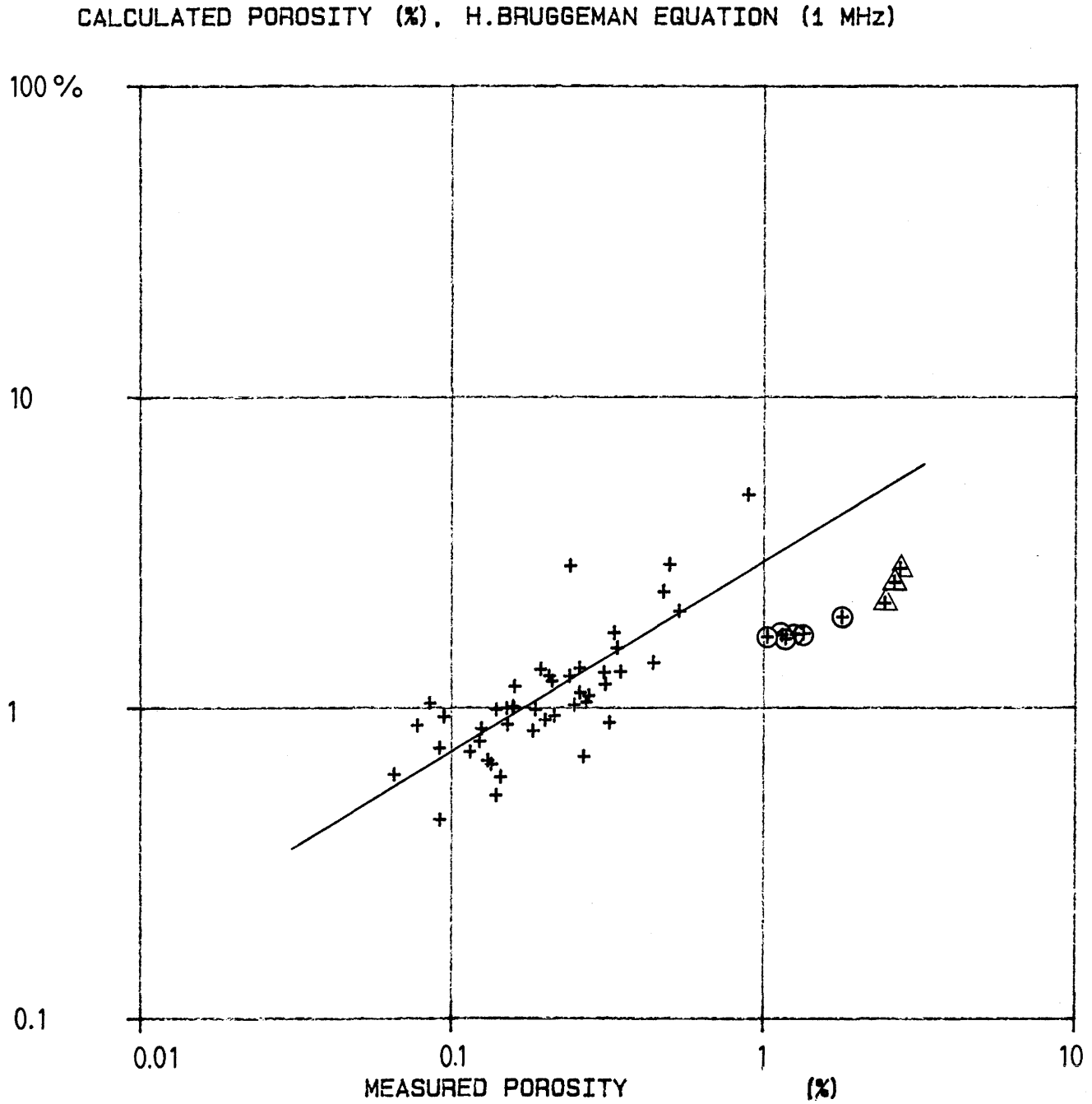

Figure 6.10 Measured immersion porosity (measured at the laboratory of the Technical University of Luleå) vs the calculated porosity according to Hanai-Bruggeman equation. All samples measured with 1 MHz frequency of the applied electric field.

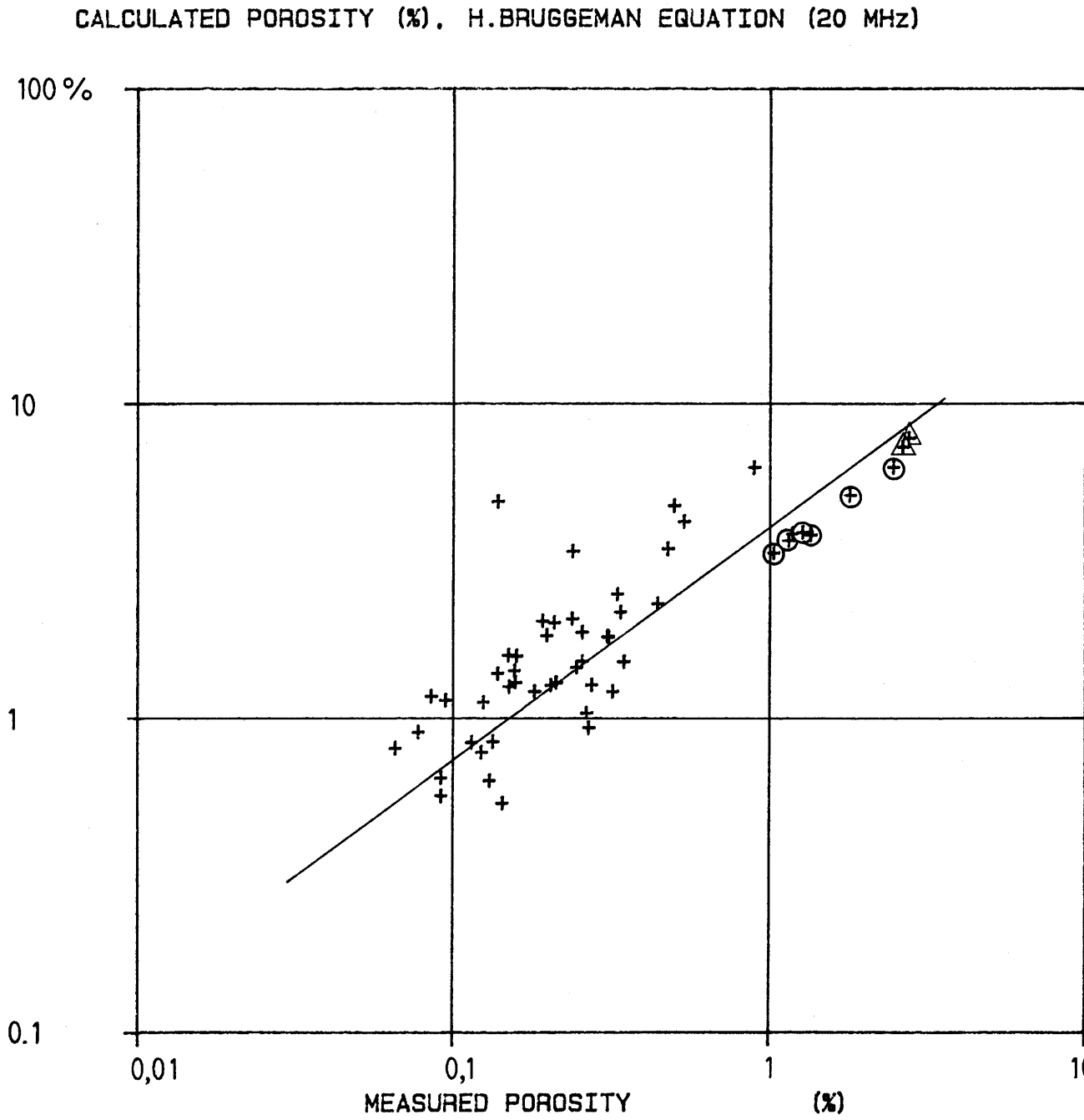

Figure 6.11 Measured immersion porosity (measured at the laboratory of the Technical University of Luleå) vs the calculated porosity according to Hanai-Bruggeman equation. All samples measured with 20 MHz frequency of the applied electric field.

Hanai-Bruggeman equation is therefore expected to result in higher porosity values. There is a rather good agreement between the calculated and measured porosity, but there are too few values with higher porosities to give a good estimate of the log-log linear relation between measured and calculated porosity (Figures 6.9, 6.10 and 6.11).

The data presented above indicate that the Hanai-Bruggeman equation gives a rather good estimate of the porosity. The Hanai-Bruggeman equation gives the best result for the depolarisation factor 0.333 and for pore water salinity and dielectric constant of about 0.1 S/m and 81, respectively. This is in agreement with the expected values of these properties.

6.3 Comparison of physical properties measured on core samples and in situ bulk properties.

The in situ measurements show that the bulk properties of the undeformed granite is more uniform compared to the major units, which are characterized by large variations in physical properties. The major units are generally more fractured than the adjacent undeformed granite. However, the degree of fracturing for each unit exhibits a large variation between the boreholes and there is thus a large variation of the fracturing over the units. The units are characterized by being the most low resistive parts in the borehole, even when the increase in fracturing is not very marked (Carlsten et. al., 1985).

The measurements on the core samples also show that the samples from the major units have a high average porosity and resistivity. The study of thin sections show strong deformation on a microscopic scale as well as on macroscopic scale. Open microfractures and cavities occur much more frequently in the major units than in the undeformed granite. This is in agreement with the in situ measured bulk properties.

The detailed study of the physical properties across units B and C in F2 presented in Chapter 4.5 shows that both resistivity measured on the samples and the logged single point resistance exhibit very similar patterns (Figure 4.13). The measured porosity also shows a similar pattern across unit B and C in F2 (Figure 4.14).

The correlation between fracture frequency and resistivity measurements both in situ and on samples and also with the porosity of the samples shows that the fracturing and the microfracturing

across for example unit B and C in F2 has a very similar pattern. This is in agreement with the fact that the major units are characterized by more intense microfracturing compared to the undeformed granite. The major units generally also show a high fracture frequency. Note that several major units have been penetrated by as many as seven boreholes (Carlsten et. al. 1985).

The high microfracturing in the rock mass and the corresponding higher porosity of the units will influence the in situ logging methods sensitive to fracturing and porosity. For example, the in situ logged resistivity measures the combined current transport through both the connected network of microfractures in the rock mass and the fractures. It is very likely that the major part of the porosity of the bedrock (the fractured rock) is caused by a network of connected microfractures. This explains the good correlation between the measured resistivity in situ and on the core samples and also the fact that intense microfracturing generally is connected with high fracturing. Thus, it is clear that the physical bulk properties such as resistivity and porosity will not only be influenced by the frequency of mapped fractures but also to a large degree by the microfracturing of the rock mass.

6.4 Comparison between the geological character and the physical properties.

The Stripa granite has been divided into undeformed granite and major units. The physical properties and geological character differ markedly between undeformed granite and major units.

The major units are characterized by a varying degree of tectonization, ranging from slightly deformed rock to breccias formed by crushing of the rock. Although these zones are well healed coherent rock they often contain cavities and are generally more fractured than the undeformed rock. They also show clear evidence of deformation on a microscopic scale. The grain matrix is more granular with several times smaller grain size than the more undeformed granite and microbreccias occur frequently. Cavities occur rather frequently in association with microbreccias. Microfractures occur frequently and often cut through and dislocate grains. The major units are also characterized by having anomalous physical properties both in situ and on core samples. They constitute the most porous and low resistive sections of the boreholes.

The undeformed granite is characterized by being a uniform and compact granite of lower fracture frequency than the major units. These parts of the granite can also on a microscopic scale be considered as a rather undeformed. Microfractures do occur in this undeformed granite but not in a large amount. They usually occur in association with grain boundaries and do not penetrate separate grains. The undeformed granite generally constitutes a uniform rock with low porosity and high resistivity, both in situ and on core samples.

The study shows that there is very good agreement between physical properties of the Stripa granite, measured both in situ and on core samples and the geological character observed both on a microscopic and a macroscopic scale.

7 CONCLUSIONS

This study of the geology and physical properties of the core samples from borehole F1 and F2 at the Crosshole site confirms that the rock mass can be divided into major units and more undeformed rock. The criteria for dividing the rock mass into these two categories is built on both the gelogical character and the physical properties as described by Carlsten et. al. (1985).

The undeformed granite is characterized by being a uniform compact granite which generally has lower fracture frequency than the major units. In the undeformed granite microfractures occur sparsely. These parts of the granite can also on a microscopic scale be considered as a rather undeformed granite.

In the major units a complex pattern of tectonization is observed. The study of thin sections shows strong deformation also on a microscopic scale. Microfractures and cavities also occur more frequently in these fractured units.

The samples from the major units have a considerably higher porosity and dielectric constant and lower resistivity than the samples from the more undeformed granite. The in situ log results presented by Carlsten et. al. (1985) clearly show that the major units are characterized by the most anomalous physical conditions.

The resistivity logged in situ and measured on samples exhibit very similar pattern of variation along the borehole. The in situ logged resistivity measures the combined current transport through both the connected net of microfractures in the rock mass and the fractures. The often rather high porosities of the cores from major units indicate that a large portion of the porosity of the bedrock (including fractures) originates from the network of microfractures. Thus it is evident that in situ measurements sensitive to the bulk porosity are often strongly influenced by the matrix porosity.

Log-log plot of the conductivity of water saturated samples versus the frequency of the applied electric field, exhibit a linear increase of the conductivity (exponent 0.38) with increasing frequency. Both samples from the major units and the undeformed granite exhibit the same linear increase, but the samples from the undeformed granite have a lower average conductivity at all measured frequencies.

The relative dielectric constant of water saturated samples decreases markedly with increasing frequency from values about 50 (major units) or 30 (undeformed granite) to low values of 5 at 50 MHz. The major units have low average dielectric constants at lower frequencies. At higher frequencies the dielectric constant is very small for both the major units and the undeformed granite and will thereby exhibit a small difference.

Measurements of the resistivity at low frequencies (1 Hz) result in low average values for the resistivity compared to measurements at 25 kHz. But from the log-log linear decrease in resistivity with increasing frequency (high frequency measurements with a Q-meter) it is evident that the resistivity should be considerably higher at low frequency. Also, the in situ measurements of the resistivity at 1 Hz at the Crosshole site result in considerably higher average resistivity than the low frequency measurements on the samples. Note that the fractures will contribute to the current transport in the in situ measurements while the current transport through the samples take place through hairline fractures and microfractures. Both the high frequency measurements and the in situ measurements indicate that the low frequency measurements result in too low values for the resistivity. The low frequency measurements are therefore probably influenced by current leakage along sample surfaces.

Archie's law which was established empirically by measurements on rock samples describes the relation between porosity and resistivity for low frequencies of the applied electric field. In this investigation the plot of measured immersion porosity against the low frequency measurement of the resisitivity has shown that the exponent in Archie's law, the so called cementation factor, is about 1.5. This study also indicates that surface conduction gives a large contribution to the total current transport.

The Hanai-Bruggeman equation relates the bulk electrical properties to the porosity for different frequencies of the applied electric field. The study by Sen et. al. (1981) has shown that Archie's law can be deduced from the Hanai-Bruggeman equation when approaching the low frequency limit. Assuming spherical particle shape Sen et. al. (1981) has shown that the exponent in Archie's law is 1.5, and the same exponent is found in this investigation.

The Hanai-Bruggeman equation gives the most reasonable results for a depolarization factor of about 0.33 which corresponds to the exponent 1.5 in

Archie's law. The best results are achieved for an assumed pore water resistivity of about 10 ohm-m or lower and for a pore water dielectric constant of 81. This is in agreement with the expected values.

The cross plot of calculated porosity according to Hanai-Bruggeman equation against measured immersion porosity shows a rather good correlation. The calculated porosities are somewhat higher than those measured on samples but also rather isolated pores, such as fluid inclusions contribute to the electrical bulk properties in high frequency measurements. The porosity calculated from the Hanai-Bruggeman equation should therefore result in higher porosity compared to the immersion porosity. The calculated porosity of Stripa granite except in the unit B is in the range between 0.3 - 6 % while the measured immersion porosity range between 0.06 - 1 %. The results show that the Hanai-Bruggeman equation can be used to describe the electrical bulk properties of the Stripa granite and that this type of mixing rule results in a good estimate of the total porosity for a heterogeneous medium.

ACKNOWLEDGEMENT

The authors wish to thank G. Agmalm who presented the data of the physical properties of the core samples in his graduate work at the Technical University of Luleå.

REFERENCES

Agmalm, G., 1985. Parametermätningar på borrkärneprover och jämförelse med borrhålsloggning från Stripa gruva. University of Luleå, Luleå, Sweden.

Carlsten, S., Magnusson, K.-Å., Olsson, O. 1985. Crosshole investigations - Description of the small scale site. Stripa Project Internal Report 85-05. SKB, Stockholm.

Carlsten, S., 1985. Hydrogeological and hydrogeochemical investigations in boreholes - Compilation of geological data. Stripa Project Internal Report 85-04. SKB, Stockholm.

Brace, W.F., Orange, A.S., 1968. Electrical resistivity changes in saturated rocks during fracture and frictional sliding. Journal of Geophysical research, 73, 1433 - 1455.

Brace, W.F., Orange, A.S. and Madden, T.R., 1965. The effect of pressure on the electrical resistivity of water saturated crystalline rocks. Journal of Geophysical research, 70, 5669 - 5678.

Duran,O., and Magnusson, K.-Å., 1984. Comparative study of geological, hydrological and geophysical borehole investigations. Technical Report 84-09, KBS, Stockholm.

Katsube, T.J., 1981. Pore structure and pore parameters that control the radionuclide transport in crystalline rocks. Proceedings of the Technical Program, International Powder and Bulk Solids Handling and Processing, Rosemont Illinois, 1981, pp 394 - 409. Cahners Exposition Group, Chicago, Illinois.

Lindblom, S., 1984. Hydrogeological and hydrogeochemical investigations in boreholes - Fluid inclusion studies in the Stripa granite. Stripa Project Internal Report 84-07. SKB, Stockholm.

Nelson, P. H., and Magnusson, K.-Å., Rachiele, R., 1982. Application of borehole geophysics at an experimental waste storage site. Geophysical Prospecting, 30, 910 - 934.

Olsson, O., Falk, L., Forslund, O., Lundmark, L., Sandberg, E. 1987. Crosshole investigations - Results from borehole radar investigations. Stripa Project Report 87-11. SKB, Stockholm.

Sen, P.N., Scala, C. and Cohen, M.H., 1981. A self-similar model for sedimentary rocks with application to the dielectric constant of fused glass beads. Geophysics, 46, 781 - 795.

Sherman, M.M., 1983. The determination of cementation exponents using high frequency dielectric measurements. The log analyst.

Waxman, M.H., and Smiths, L.J.M., 1968. Electrical conductivities in oil-bearing shaly sand. Soc. Petr. Eng. journal. 8, 107 - 122.

Öquist, U., 1981. Measurements of electrical properties of rocks and its application to geophysical investigations of ores and waste disposals. Doctoral thesis, Kungliga Tekniska Högskolan, Stockholm.